An Updated Review of Atmospheric Mercury

Seth N. Lyman,[a,b] Irene Cheng,[c] Lynne E. Gratz,[d] Peter Weiss-Penzias,[e,f] Leiming Zhang[c]

[a]Bingham Research Center, Utah State University, 320 N Aggie Blvd., Vernal, Utah, U.S.A.

[b]Department of Chemistry and Biochemistry, Utah State University, 4820 Old Main Hill, Logan, Utah, U.S.A.

[c]Air Quality Research Division, Environment and Climate Change Canada, 4905 Dufferin St., Toronto, Ontario, Canada

[d]Environmental Studies Program, Colorado College, 14 East Cache la Poudre St., Colorado Springs, CO, U.S.A.

[e]Chemistry and Biochemistry Department, University of California, Santa Cruz, 1156 High St, Santa Cruz, California, U.S.A.

[f]Microbiology and Environmental Toxicology Department, University of California, Santa Cruz, 1156 High St, Santa Cruz, California, U.S.A.

*Corresponding author, seth.lyman@usu.edu, +14357221740

ABSTRACT

The atmosphere is a key component of the biogeochemical cycle of mercury, acting as a reservoir, transport mechanism, and facilitator of chemical reactions. The chemical and physical behavior of atmospheric mercury determines how, when, and where emitted mercury pollution impacts ecosystems. In this review, we provide current information about what is known and what remains uncertain regarding mercury in the atmosphere. We discuss new ambient, laboratory, and theoretical information about the chemistry of mercury in various atmospheric media. We review what is known about mercury in and on solid- and liquid-phase aerosols. We present recent findings related to wet and dry deposition and spatial and temporal trends in atmospheric mercury concentrations. We also review

atmospheric measurement methods that are in wide use and those that are currently under development.

GRAPHICAL ABSTRACT

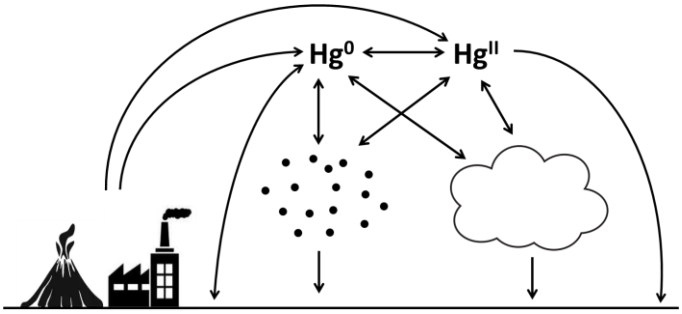

KEYWORDS

chemistry, deposition, gas-particle partitioning, oxidized

1. Introduction

Mercury is a potent toxicant that impacts human (Bernhoft, 2012; Houston, 2011; Mergler et al., 2007) and environmental health (Henny et al., 2002; Spry and Wiener, 1991; Warnick and Bell, 1969; Wright et al., 2018). Although exposure of humans and wildlife to toxic levels of mercury typically occurs through consumption of contaminated food (Castro-González and Méndez-Armenta, 2008; Oken et al., 2005), most anthropogenic mercury pollution is emitted into the atmosphere and enters ecosystems via atmospheric deposition (Driscoll et al., 2013). Emitted gas-phase elemental mercury, which is relatively

inert, can be transported globally (Ebinghaus et al., 2009; Sprovieri et al., 2016; Sprovieri et al., 2010) before it is taken up by plants (Wright et al., 2016) or soils (Gustin et al., 2008) or oxidized in the atmosphere (Jiao and Dibble, 2017a; Lam et al., 2019; Shah et al., 2016). Emissions of oxidized mercury compounds have a more local impact than elemental mercury (Fu et al., 2015; Weiss-Penzias et al., 2011), because they are more reactive, more water-soluble, and thus, deposit more quickly (Lin et al., 2006). Chemical and physical transformations of atmospheric mercury are often reversible. In some atmospheric environments, including polar spring (Steffen et al., 2015), the upper atmosphere (Lyman and Jaffe, 2012; Slemr et al., 2018), and perhaps polluted urban areas (Chen et al., 2016), elemental mercury can become oxidized relatively quickly. Once oxidized, mercury compounds dynamically partition between the gas and aerosol phases (Amos et al., 2012; Cheng et al., 2014). Furthermore, they are readily reduced back to elemental mercury from either phase (Landis et al., 2014; Saiz-Lopez et al., 2018) and, at least in cloud and fog water, can undergo a variety of other chemical transformations (Li et al., 2018; Lin and Pehkonen, 1999). The concentrations and speciation of mercury in the atmosphere depend on proximity to sources (Fu et al., 2015), availability of oxidants (Obrist et al., 2011), aerosol concentrations and properties (Malcolm et al., 2009), regional and global-scale meteorology (Holmes et al., 2016), and surface conditions (Jiskra et al., 2018).

Ultimately, the fate of all mercury emitted to the atmosphere is to deposit to ecosystems. Elemental mercury exchanges dynamically with plant stomata and soils (Eckley et al., 2011; Howard and Edwards, 2018; Obrist et al., 2017; Yu et al., 2018). Oxidized mercury compounds, whether in the gas or aerosol phase, can be taken up by atmospheric water (Sheu and Lin, 2011; Zhou et al., 2018a) and deposited in precipitation (Kaulfus et al., 2017; Zhou et al., 2018a) or undergo dry deposition to terrestrial and aquatic surfaces (Sather et al., 2013; Wright et al., 2016). Mercury deposited to the terrestrial environment can cause environmental harm as it is transported to aquatic systems (Faïn et al., 2011; Grigal, 2002). In the aquatic environment, it can be methylated (Heyes et al., 2006; Monperrus et al.,

2007) and then bioaccumulated and biomagnified in the aquatic food chain (Hammerschmidt and Fitzgerald, 2006; Schwindt et al., 2008). Human or animal consumption of high trophic-level fish (Bernhoft, 2012) or other foods that have been contaminated with mercury (Barrett, 2010; Li et al., 2010; Li et al., 2012; Zhang et al., 2010; Zhao et al., 2019) can lead to toxic effects.

The purpose of this work is to present an updated review of the behavior and chemistry of mercury in the atmosphere. Many reviews have already been published that cover various aspects of this topic. These are referenced in the relevant sections below. Our goal is to provide updates and additions to, rather than a reproduction of, these existing reviews and to underscore areas where uncertainty or lack of consensus exists. We focus in particular on gas and aerosol phase chemistry, atmospheric deposition, spatial and temporal trends, and measurement methods.

Some topics and sub-topics discussed herein contain more depth because they have not, to our knowledge, been reviewed before. For other topics, we only provide overviews and highlights, since extensive reviews already exist. Except in the context of its relation to spatial and temporal trends (Section 4), we do not discuss emissions to the atmosphere, since this will be the subject of a separate article in this issue.

Acronyms and abbreviations in the atmospheric mercury literature have been used inconsistently. We use chemical formulas in this work wherever possible to avoid confusion. Oxidized mercury measurements contain bias and are largely operationally-defined (Section 5.2.2), however, so we use the less-specific acronyms GOM (gas-phase oxidized mercury) and PBM (particulate-bound mercury) when describing these measurements. We use Hg^{II} or full chemical formulas instead when certainty exists about chemical formulas or oxidation states. We use Hg^{2+} when discussing oxidized mercury compounds or ions in the aqueous phase.

Atmospheric mercury concentrations are typically reported in units of ng or pg m^{-3}, with the volume measurement made at IUPAC standard conditions (Nic et al., 2005). We follow this convention in this work.

Also, it remains unclear whether Tekran 2537 and similar mercury analyzers without upstream processing equipment measure total gas-phase mercury or only elemental mercury. Thus, these measurements are also operationally defined. We use the acronym GEM (gas-phase elemental mercury) to describe them, though they likely include GEM and some portion of Hg^{II} compounds that exist in the atmosphere, and the amount of Hg^{II} they include likely depends on the sampling configuration and the chemical and physical conditions of the atmosphere. Also, when KCl denuders are used upstream of elemental mercury analyzers, some of the captured Hg^{II} is reduced to elemental mercury and measured in that form (Lyman et al., 2010). Some have used the acronym TGM (total gaseous mercury), rather than GEM, but, to our understanding, no information exists about the percentage of gas-phase Hg^{II} that is analyzed by elemental mercury analyzers with an upsteam KCl denuder or without upstream sample processing. Many have asserted that this issue is inconsequential, because atmospheric Hg^{II} concentrations are low relative to Hg^0 (Ci et al., 2011; Fu et al., 2012a), but this assertion has been shown to be inaccurate in some environments (Fu et al., 2015; Obrist et al., 2011; Swartzendruber et al., 2006; Weiss-Penzias et al., 2009), especially when the low bias in KCl-denuder based GOM measurements is taken into account (Huang et al., 2013; Lyman et al., 2016). Thus, while we use the acronym GEM to describe these measurements, we acknowledge that it doesn't describe most measurements reviewed herein with complete accuracy. See Section 5 for more information.

2. Gas and Particle-phase Chemistry

Si and Ariya (2018) reviewed the recent advances in atmospheric mercury chemistry, considering efforts to determine Hg^0 oxidation pathways, aqueous reduction of Hg^{II} compounds, and heterogeneous

mercury chemistry. Other relevant and recent reviews include Durnford and Dastoor (2011), Subir et al. (2011), Subir et al. (2012), Gustin et al. (2015), Ariya et al. (2015), and Mao et al. (2016). Diagrams of many of the relevant processes are available in Subir et al. (2011) and Si and Ariya (2018).

2.1. Gas-phase Oxidation

Elemental mercury oxidation is a key facet of the mercury biogeochemical cycle, given the relative lifetimes and solubility of mercury in its different forms. Hg^0 persists in the atmosphere long enough to be transported globally, whereas Hg^{II} compounds are generally more water-soluble and thus more readily removed from the atmosphere through wet and dry deposition (Driscoll et al., 2013). As such, the conversion from Hg^0 to Hg^{II} plays a key role in atmospheric and biogeochemical Hg cycling. Yet, questions remain as to the dominant oxidation pathway(s) in the atmosphere, largely due to uncertainties around the kinetics associated with proposed mechanisms, an inability to determine the chemical form of GOM in ambient air, and the validation of chemical models against measurements made with known interferences (Obrist et al., 2018; Si and Ariya, 2018). Here we review the proposed oxidation pathways, considering the most recent studies to report on their kinetics and viability to contribute to ambient mercury chemistry. Tables summarizing the latest kinetics on gaseous mercury redox chemistry are provided in Subir et al. (2011) and Si and Ariya (2018), including experimentally- or theoretically-determined rate constants for each reaction and citations for the work that determined them.

2.1.1. O_3 / OH

Oxidation by O_3 and OH were once widely assumed to be the dominant oxidation mechanisms for ambient Hg^0 (Calvert and Lindberg, 2005). These mechanisms continue to be routinely employed in chemical models used to investigate mercury cycling and deposition (Cohen et al., 2016; De Simone et

al., 2017; Pacyna et al., 2016). Several publications have reported the associated kinetics for oxidation by O_3 (Hall, 1995; Pal and Ariya, 2004b; Rutter et al., 2012; Snider et al., 2008) and OH (Miller et al., 2001; Pal and Ariya, 2004a; Sommar et al., 2001), with a range of rate constants determined at atmospherically relevant conditions (Si and Ariya, 2018). Some have argued, however, that these reactions are irrelevant in the ambient atmosphere (Calvert and Lindberg, 2005; Hynes et al., 2009). Recent work on Hg^0 oxidation by O_3 and OH has focused on the incorporation of these mechanisms and their associated kinetics into chemical models and the validation of model output against available measurements, which has continued to inform the role that O_3/OH oxidation may play in the atmosphere (Section 2.1.4).

2.1.2. Bromine

Bromine-initiated oxidation has been given a great deal of attention in the last decade as another important gas-phase mechanism. Br oxidation is thought to proceed by a two-step mechanism, in which gaseous Hg^0 reacts with photolytically-produced atomic Br to produce the unstable product HgBr that can either dissociate back to Hg^0 or react with other species (such as Br, OH, BrO, HO_2, or NO_2) to form inorganic Hg^{II} compounds (Dibble et al., 2012; Dibble and Schwid, 2016; Goodsite et al., 2004; Holmes et al., 2010; Horowitz et al., 2017; Jiao and Dibble, 2017b). The experimentally- and theoretically-determined reaction rate constants for this mechanism also vary widely (Si and Ariya, 2018; Subir et al., 2011), and a range of rate constants have been used (Shah et al., 2016). Naturally, the chemical form of the resulting Hg^{II} compound is dependent on the radical species that participates in the second step of the reaction, but at this time no method exists to determine the chemical composition of GOM. Wang et al. (2014a) argued that NO_2 and HO_2 could carry out the second step of the Br-induced oxidation pathway in the marine boundary layer. The reaction of HgBr with NO_2 is proposed to produce either $BrHgNO_2$ or BrHgONO, while the reaction of HgBr with HO_2 produces $BrHgHO_2$. The kinetics of these

secondary reactions were recently investigated for the first time using computational chemistry by Jiao and Dibble (2017a).

2.1.3. Other Potential Oxidants: Cl, H_2O_2, and NO_3

While most recent work has focused on O_3, OH, and Br-induced oxidation chemistry, a small number of other oxidants have also been proposed (Pacyna et al., 2016; Si and Ariya, 2018). Cl-initiated Hg^0 oxidation likely also proceeds by a two-step mechanism with HgCl as the intermediate that is oxidized in the second step by NO_2, HO_2, ClO, or BrO (Sun et al., 2016). Tokos et al. (1998) provided laboratory measurements of the rate constant for gaseous Hg^0 oxidation by hydrogen peroxide (H_2O_2). The nitrate radical (NO_3) has also been proposed as a potential oxidant of Hg^0 (Gustin et al., 2013; Lin and Pehkonen, 1999; Peleg et al., 2015). Hynes et al. (2009) suggested the reaction is highly endothermic and not atmospherically viable, while Dibble et al. (2012) used theoretical calculations to suggest that NO_3 does not form strong bonds with Hg^0 and thus is unlikely to initiate gas-phase oxidation. While NO_3 may not be capable of initiating Hg^0 oxidation, Si and Ariya (2018) posited that it could be involved in the secondary reaction of Hg^I to Hg^{II} that is initiated by another oxidant such as Br or OH. Due to large uncertainties around the kinetics of these other oxidation mechanisms and/or questions of atmospheric viability, these mechanisms have not been as thoroughly investigated in chemical modeling studies.

2.1.4. Are Bromine Radicals the Globally Dominant Oxidant?

The idea that there may be a globally-dominant oxidation mechanism for atmospheric mercury remains a disputed topic in the mercury research community, largely due to uncertainties around reaction kinetics and a lack of reliable measurements with high spatiotemporal coverage accompanied by measurements of potentially relevant oxidants (Obrist et al., 2018; Pacyna et al., 2016; Si and Ariya, 2018; Travnikov et al., 2017). As noted above, oxidation of Hg^0 by O_3 and OH remains a common

pathway in many global and regional chemical models (De Simone et al., 2014; Gencarelli et al., 2017; Kos et al., 2013; Pacyna et al., 2016). Though the gas-phase reaction of Hg^0 with these oxidants was also suggested to be too slow to act as the dominant oxidation mechanism in the atmosphere (Driscoll et al., 2013; Hynes et al., 2009; Subir et al., 2011), some recent modeling studies have still found good agreement with observed ambient GEM and mercury wet deposition when employing these mechanisms (Travnikov et al., 2017; Weiss-Penzias et al., 2015).

On the other hand, Holmes et al. (2010) proposed that Br-induced oxidation is the globally-dominant oxidation pathway, and some global models have continued with this assumption (Amos et al., 2012; Horowitz et al., 2017). The Br-induced oxidation mechanism has been observed with measurements and chemical models to drive gaseous mercury oxidation in certain environments, including the marine boundary layer (Holmes et al., 2009; Wang et al., 2014a), the tropical and subtropical free troposphere (Gratz et al., 2015a; Shah et al., 2016), in polar regions (Brooks et al., 2006; Goodsite et al., 2004; Jiao and Dibble, 2017b; Steffen et al., 2008), and over the Dead Sea (Obrist et al., 2011) where halogen species such as Br are abundant. It remains less clear what role this mechanism plays in the continental free troposphere or boundary layer.

Several recent regionally-focused papers have attempted to address the question of a dominant mercury oxidant. Ye et al. (2016) used a chemical box model to simulate ambient mercury concentrations at marine, coastal, and inland sites in the Eastern United States. They found Br-initiated oxidation to be important at the marine site, but O_3/OH oxidation to better explain observations at coastal and inland sites. They also suggested the possibility of nighttime H_2O_2 oxidation at the inland site. Weiss-Penzias et al. (2015) applied the GEOS-Chem global chemical model alternately with the Br mechanism and O_3/OH mechanism to ambient mercury measurements from several high elevation sites (four in the western United States and one in Asia) and found varying results, in part concluding that

neither mechanism alone could accurately explain the observations. Wang et al. (2014a) concluded that while Br was the primary oxidant in the marine boundary layer, neither oxidation by Br nor by O_3/OH alone could reproduce observations.

In a comparative modeling study, Travnikov et al. (2017) sought in part to identify the role of the aforementioned oxidation pathways. They found that the Br mechanism was able to reproduce the observed seasonal variation in the GOM-to-GEM ratio in the near-surface layer, but did not accurately simulate the timing of seasonal wet deposition patterns in North America and Europe. In contrast, OH-driven oxidation alone simulated the range and amplitude in mercury observations but shifted the seasonal variability, and the O_3 mechanism alone did not simulate significant seasonal variability as is seen in observations. These results suggested the possibility for more complex oxidation chemistry and multiple oxidation pathways in different parts of the atmosphere and under different atmospheric conditions (Travnikov et al. (2017). Field studies that utilized thermal desorption methods have come to similar conclusions (Gustin et al., 2016; Huang et al., 2017).

Given this recent work, the idea of a globally dominant oxidant remains in question. In fact, the leading train of thought now appears to lean more toward the notion that gaseous mercury oxidation is carried out by more complex chemical mechanisms and multiple oxidation pathways (in the gas phase and on surfaces) that become more or less dominant by location and season (Pacyna et al., 2016; Travnikov et al., 2017; Wang et al., 2015; Weiss-Penzias et al., 2015). It may, for example, be the case that the O_3/OH mechanism is still relevant in certain environments (such as the continental boundary layer) even though uncertainties in the associated kinetics and atmospheric viability remain, while the Br-induced mechanism dominates in other environments such as the marine boundary layer, the subtropical free troposphere, and polar regions; alternatively or additionally, there may be a two-step mechanism

initiated by one oxidant but carried forward by a different species depending on the location and/or time of year (Horowitz et al., 2017; Pacyna et al., 2016; Si and Ariya, 2018; Travnikov et al., 2017).

An underlying source of uncertainty in all of these studies is that most of the work done to determine the relevant oxidation pathways comes from chemical modeling work, wherein the included chemical reactions have large and varying uncertainties around their associated kinetics (Si and Ariya, 2018). Moreover, those model outputs are being compared predominantly with surface observations of GOM that have known low bias due to interferences from O_3 and water vapor (Gustin et al., 2015; Jaffe et al., 2014; Lyman et al., 2010; McClure et al., 2014). These circumstances undoubtedly limit the current ability to ascertain the chemical mechanisms that govern mercury oxidation on local, regional, or global scales.

2.1.5. Chemical Composition of Gaseous Oxidized Mercury

Another limitation in the current understanding of gaseous mercury chemistry is a lack of knowledge about the chemical form(s) of GOM in the atmosphere. Current ambient air measurement techniques operate by quantifying total GOM or by separating the gaseous from the particle-bound forms of oxidized mercury, but the actual molecular forms of oxidized mercury cannot currently be distinguished. Ambient GOM is believed to exist as Hg^{II}, with the assumption that Hg^{I} compounds are highly unstable and thus reduces back to Hg^0 or is further oxidized to Hg^{II}. Recent work using the University of Nevada Reno Reactive Mercury Active System (UNRRMAS), which collects GOM onto nylon or cation exchange membranes that are later analyzed by thermal desorption, has identified Hg^{II} compounds in ambient air that match the thermal desorption patterns of $HgBr_2$, $HgCl_2$, HgO, $Hg(NO_3)_2$, and $HgSO_4$ (Gustin et al., 2016; Huang et al., 2017). A study that used this method in Nevada found a prevalence of thermal desorption profiles that match halogen-containing species at a high-elevation site, nitrogen- and oxygen-containing species at an urban site (Gustin et al., 2016). This method currently requires

sampling onto membranes for 1-2 weeks to collect sufficient sample for analysis, making source or air mass characterization challenging. Also, the possibility exists that mercury or membrane chemistry changes during sampling, impacting thermal desorption results, and overlapping desorption profiles have the potential to be misinterpreted (Though work to answer these questions is underway. See Gustin et al. (2019)). Jones et al. (2016) and Deeds et al. (2015) have developed mass spectrometry systems to identify oxidized mercury compounds. Both groups successfully identified mercury halides in laboratory tests, but identification in ambient air has proven more difficult.

2.2. Gas and Aerosol-phase Reduction

Hg^{II} reduction has been reported in coal-fired power plant plumes (Edgerton et al., 2006; Landis et al., 2014), and on particle surfaces, including clouds and aerosols with many different chemical compositions (Ariya et al., 2015; Horowitz et al., 2017; Subir et al., 2012; Tacey et al., 2016; Tong et al., 2013; Tong et al., 2014). Aqueous chemical reactions can occur on or within solid or liquid aerosols, including mercury complex formation, and some of these reactions may allow mercury to be reduced to the elemental form. In the aqueous phase, Hg^{2+} forms complexes with various ligands, such as sulfite, chloride, and other halides. In the presence of UV, some Hg^{2+} complexes can undergo photoreduction (Subir et al., 2012; Ariya et al., 2015). Malcolm et al. (2007) suggested that particle-to-gas partitioning via reduction of Hg^{II} played a role in the loss of mercury collected on filter pack samples due to exposure of the filter packs to acidic gases and high relative humidity conditions in coastal environments. Under these conditions, Hg^{2+} forms complexes with sulfite in the aqueous phase that dissociates rapidly to Hg^{+} and then is lost as Hg^{0}. More information about mercury chemistry in the atmospheric aqueous phase is given in Section 2.6.

The inclusion of reduction processes in models has resulted in improved simulations of surface concentrations and deposition fluxes (de Foy et al., 2016; Holmes et al., 2010; Lohman et al., 2006; Pongprueksa et al., 2008; Zhang et al., 2012c). Many current chemical transport models assume that Hg^{2+} reduction occurs in the aqueous phase within clouds (Horowitz et al., 2017; Shah et al., 2016). However, a recent study looked at photoreduction pathways of atmospheric Hg^{II} compounds, showing that irradiation experiments with rainwater do not support fast aqueous-phase Hg^{II} photoreduction (Saiz-Lopez et al., 2018). In related work, Sitkiewicz et al. (2016) and Sitkiewicz et al. (2019) calculated absorption cross-sections for many mercury compounds. Saiz-Lopez et al. (2018) suggest that arbitrarily scaling up aqueous photolytic reduction rates (Horowitz et al., 2017) is inappropriate since measured photoreduction rates in atmospheric water are low. Using calculated absorption cross-sections to infer the corresponding gas-phase photoreduction rates for the main mercury compounds thought to be in the atmosphere, Saiz-Lopez et al. (2018) and Saiz-Lopez et al. (2019) show that fast gas-phase photolysis of Hg^{I} intermediates and Hg^{II} compounds dominates atmospheric mercury reduction and leads to a factor-of-two increase in the modeled global atmospheric mercury lifetime. They further postulate that relatively low photoreduction rates for HgBrOH and $HgBr_2$ allow these compounds to dominate atmospheric Hg^{II} composition.

2.3. Heterogeneous Oxidation

Subir et al. (2012) and Ariya et al. (2015) suggested that the importance of heterogeneous chemistry in atmospheric mercury cycling, including heterogeneous oxidation, has been underappreciated and understudied. Gustin et al. (2013) suggested that heterogeneous reactions with aerosols and/or manifold walls could explain oxidized mercury behavior during the RAMIX measurement intercomparison study. It is well known that Hg^0 can be oxidized and undergo complex chemical transformations in the aqueous phase, likely on deliquesced particulate matter as well as on cloud and

fog droplets (see Sections 2.2 and 2.6), but we discuss here the possibility of oxidation on aerosols more generally. Many have argued that gas-phase mercury oxidation by O_3 is unlikely to occur in the atmosphere (Section 2.1.1), but Calvert and Lindberg (2005) argued that the process could be favorable if mediated by particle surfaces (see also Seigneur et al. (2006)). It is also possible that Hg^0 or unstable Hg^I compounds could come in contact with aerosol surfaces, and that the aerosol surfaces could mediate an oxidation reaction. The supposed product of the reaction of O_3 with Hg^0 is HgO (Pal and Ariya, 2004b), and because this compound is not volatile (Lin and Pehkonen, 1999), the reaction proposed by Calvert and Lindberg would lead to an increase in particle-bound mercury. If a different reaction led to the formation of more volatile Hg^{II} compounds, those compounds could subsequently transfer into the gas phase (Section 2.4). To our knowledge, this idea is completely theoretical, with no field or laboratory studies showing conclusive evidence of aerosol-mediated mercury oxidation reactions. Such studies are called for.

2.4. Gas-Particle Partitioning

In addition to primary emissions of particles that contain mercury, particulate-bound mercury can form when gas-phase mercury can sorb to particles in the ambient atmosphere. While adsorption of Hg^0 to particulate matter is believed to be negligible, gas-particle partitioning occurs for semi-volatile gas-phase Hg^{II} (Seigneur et al., 1998). This partitioning process is dependent upon several factors, including the air temperature, particle composition, and the existence of an aerosol aqueous phase.

2.4.1. Temperature dependence

Since Hg^{II} compounds are non-volatile or semivolatile (Lin and Pehkonen, 1999; Lin et al., 2006), they partition to the particle phase at low temperatures and shift to the gas phase at high temperatures. Several studies have derived gas-particle partitioning models for Hg^{II} as a function of air temperature. A

linear regression model was previously used to develop gas-particle partitioning relationships for other semi-volatile organic compounds, e.g., PAHs (Pankow, 1991; Pankow, 1992), and is expressed as follows:

$$Log(1/K_p) = a + b(1/T)$$

K_p is a partition coefficient that quantitates the gas-particle partitioning of Hg^{II}, T is the temperature in Kelvin, and *a* and *b* are the y-intercept and slope, respectively. K_p has been computed as shown below using PBM, GOM and total particulate matter (Rutter and Schauer, 2007a; Rutter and Schauer, 2007b) or particulate matter less than 2.5 μm in aerodynamic diameter ($PM_{2.5}$) (Amos et al., 2012; Cheng et al., 2014), as:

$$K_p = \frac{PBM/TPM}{GOM}$$

where TPM is total particulate matter. While K_p is the most common gas-particle partitioning parameter, another measure of gas-particle partitioning is the fraction of PBM in total oxidized mercury (GOM+PBM) (Cheng et al., 2014), which was adopted from gas-particle partitioning models of water-soluble organic compounds (Hennigan et al., 2008).

As shown in Table 1, the slopes and y-intercepts of gas-particle partitioning equations vary among sampling locations. The slope can be sensitive to the aerosol composition, and variation in the y-intercept may be due to differences in particle sizes and number concentrations (Rutter and Schauer, 2007a). Because GOM measurements are biased low, and because the extent of the bias changes with atmospheric conditions (Lyman et al., 2016; McClure et al., 2014), the values in Table 1 are likely to contain bias.

Table 1: Temperature-dependent gas-particle partitioning models for Hg^{II}. K_p is the gas-particle partition coefficient and T is the temperature in Kelvin.

Model	Type of data	Reference
$Log(1/K_p) = 15 - 4250(1/T)$	Field data from 1 site	Rutter and Schauer (2007a)
$Log(1/K_p) = 10 - 2500(1/T)$	Field data from 5 sites	Amos et al. (2012)
$Log(1/K_p) = 12.7 - 3485.3(1/T)$	Field data from 2 sites	Cheng et al. (2014)
$Log(1/K_p) = 13.5 - 3362.7(1/T)$	Field data from 1 site	Lee et al. (2016)
$Log(1/K_p) = 12 - 3092(1/T)$	Field data from 1 site	Zhang et al. (2017b)
$Log(1/K_p) = 19 - 5720(1/T)$	Lab-generated ammonium sulfate	Rutter and Schauer (2007a)
$Log(1/K_p) = 9 - 2780(1/T)$	Lab-generated adipic acid aerosols	Rutter and Schauer (2007a)

In many chemical transport models, Hg^{II} is assumed to exist completely in the gas phase or as an arbitrary percentage split between the gas and particle phases (Amos et al., 2012; Holmes et al., 2010; Lei et al., 2013). Gas-particle partitioning models derived from field measurements can produce K_p values that are, in most cases, similar to measured values (Cheng et al., 2014). Large discrepancies between predicted and observed K_p have been found at sites impacted by point sources, where other factors may influence the partitioning between GOM and PBM, such as emissions speciation and chemical composition of emitted aerosols (Cheng et al., 2014; Rutter and Schauer, 2007a; Rutter and Schauer, 2007b). Model simulations by Vijayaraghavan et al. (2008) that used the temperature-dependent gas-particle partitioning model developed by Rutter and Schauer (2007a) showed that the fraction of Hg^{II} partitioned to particles was 23% on average (ranging from 10-80%) with higher fractions in the western and midwestern United States due to colder temperatures and/or higher particulate concentrations (Vijayaraghavan et al., 2008). Another gas-particle partitioning model was derived and introduced into the GEOS-Chem model (Amos et al., 2012). Simulated Hg^{II} was present mostly in the gas-phase (>90%) in warm air and was only about 10% in the gas phase in cold air.

2.4.2. Dependence on Aerosol Composition

Aside from temperature, the chemical composition of aerosols and the presence or absence of an aerosol aqueous phase affect the gas-particle partitioning of Hg^{II}. In an experimental study, K_p values were measured for various synthetically-produced dry atmospheric aerosols, including $NaNO_3$, NaCl, KCl, ammonium sulfate, levoglucosan, and adipic acid (Rutter and Schauer, 2007b). Large K_p values were observed for $NaNO_3$, NaCl, and KCl, which indicates Hg^{II} tends to remain in the particle phase on those surfaces. Small K_p values were found for ammonium sulfate, levoglucosan, and adipic acid, with an estimated 50% of the Hg^{II} partitioning to the gas phase. Depending on the particle composition, K_p ranged from 1-900 $m^3\ \mu g^{-1}$ (Rutter and Schauer, 2007b). The large partition coefficient for NaCl particles was also confirmed in another experimental study, which tested the removal efficiency of ambient air GOM and $HgCl_2$ by NaCl-coated sampling denuders (Malcolm et al., 2009). The results showed that NaCl- and sea salt-coated denuders were able to remove 88-100% as much GOM in an air stream as KCl-coated denuders. This suggests that Hg^{II} is efficiently scavenged by sea salt aerosols and is likely an important sink for Hg^{II} at marine sites (Malcolm et al., 2009). Measurements of PBM using cascade impactors in coastal and marine sites also found a large proportion of particulate mercury in coarse particles, which consist mostly of sea salt (Feddersen et al., 2012).

Due to the solubility of GOM, the presence of an aerosol aqueous phase facilitates the uptake of GOM to aerosols. This process has been described in several modeling studies conducted in the marine boundary layer. Holmes et al. (2009) derived an algorithm to estimate the uptake of GOM by sea salt aerosols in the aqueous phase. The scheme assumed Hg^{2+} forms aqueous complexes with chloride. They used a mass transfer equation to describe the net flux of $HgCl_2$ and chloride complexes from the gas to the aerosol aqueous phase. Their equation takes into account particle growth relative to the radius of a dry particle. In another box model, the uptake of additional GOM species other than chloride

were also estimated using this mass transfer approach (Ye et al., 2016). Aerosol liquid water content has a strong effect on the partitioning of GOM to the aerosol aqueous phase (Hedgecock et al., 2003; Ye et al., 2016). This is further supported by other studies showing that increased water uptake by aerosols drives the partitioning of water-soluble gases to the aerosol aqueous phase (Carlton and Turpin, 2013; Hennigan et al., 2008).

Aqueous chemical reactions complicate gas-particle partitioning behavior and are discussed in Sections 2.2 and 2.3. The uptake of GOM by sea salt aerosols reduces GOM concentrations in the marine boundary layer, according to model simulations. Selin et al. (2007) showed that one-third of global mercury dry deposition is attributed to Hg^{II} compounds sorbed to sea salt. This process was also necessary for the model to reproduce the low GOM concentrations typically observed in marine environments. In another modeling study, it was estimated that almost all the Hg^{II} in the marine boundary layer was associated with sea salts (Holmes et al., 2009). In this study, sea salt uptake followed by deposition comprised 65-80% of the total deposition of Hg^{II} at marine boundary layer sites, whereas direct deposition accounted for up to 15%.

2.5. Particle-phase Size Distribution

Generally, mercury in fine particles (< 2.5 μm in diameter) is formed by sorption of gaseous Hg^{II} during or after condensation and coagulation of combustion products, while PBM in coarse particles (> 2.5 μm) is formed through the sorption of gaseous Hg^{II} onto naturally generated particles, such as salt spray, dust, and mechanical processes from anthropogenic sources (Chen et al., 2016; Mamane et al., 2008). Because fine particles dominate the surface area of all particles in the atmosphere, it is generally accepted that the majority of PBM resides in fine particles (Feddersen et al., 2012). In recent years, size-resolved PBM measurements have been collected, usually using multi-stage impactors that collect size

fractions between 0.1 and 18 μm in diameter. Table 2 summarizes the results of these measurements in both heavily polluted urban, mildly polluted suburban, and cleaner background air. Section 5 reviews possible biases in these measurements. To our knowledge, size-fractionated PBM measurements have not been reviewed in this way before.

Table 2: Summary of particle size-resolved measurements of PBM

Location	Period	Total PBM (pg m^{-3})	Size fraction with highest concentration of PBM (μm)	Composition of particle in size fraction with highest PBM concentration	Reference
Beijing, China	All year, 2016-17	297.9 ± 340.4	0.56–1	75-87% of total found in 0.05-2.0 μm size fraction	Tang et al. (2019)
Shanghai, China	Spring, 2017	318 ± 144	0.56 – 1.0	63.3% of total found in 0.05-2.0 μm size fraction	Han et al. (2018)
Shanghai, China	Winter, 2013-14	4110 ± 530[a] 1340 ± 150[b]	0.56 – 1.0[a] 0.18 – 0.32[b]	32 pg μg^{-1} [a] 20 pg μg^{-1} [b]	Chen et al. (2016)
Shanghai, China	All Year, 2013	1270 ± 716[a] 341 ± 187[b]	< 2.5	10.7 pg μg^{-1} [a] 7.4 pg μg^{-1} [b]	Chen et al. (2016)
Shanghai, China	Selected times, 2004-07	560 ± 220	1.6 – 3.7	3.07 pg μg^{-1}	Xiu et al. (2009)
Seoul and Chuncheon, South Korea	Winter and summer, 2009-10	6.8 ± 6.5	0.18 – 0.32 at both urban and rural sites, both summer and winter	0.47 pg μg^{-1} (urban, winter) 0.50 (rural, winter) 0.87 (urban, summer) 0.65 (rural, summer)	Kim et al. (2012)
Central Taiwan	Fall, 2010	297	< 1	0.913 ± 441 pg μg^{-1} (industrial site)	Chen et al. (2012)
Taiwan	July-December 2018	48.8 ± 23.4	Coarse		Fang et al. (2019)
South China Sea	Fall 2015	3.2 ± 1.8	5.8 - 9.0		Chen et al. (2012); Wang et al. (2019)
Coastal Taiwan	Fall 2009-Winter 2010	70	2.5 - 10	0.003-0.004 pg μg^{-1} (suburban site)	Fang et al. (2010); also see Fang et al. (2012)
Coastal Maine	Winter and summer, 2009-10	5	3.3 – 4.7 summer 0.7 – 1.1 winter	60% of total PBM in summer found in 1.1 to 5.8 μm size fractions. 65 % of total PBM in winter found in < 1.1 μm size fraction.	Feddersen et al. (2012)
Central Poland	April 2013-October 2014	7.3 – 22.6	> 2.2	Coarse PBM concentration was 3.1 x higher than fine PBM	Siudek et al. (2016)

[a]Haze days in Shanghai, with mean PM10 of 240 mg m^{-3}

[b]Non-haze days in Shanghai, with mean PM10 of 60 mg m^{-3}

Table 2 shows that in polluted air, such as in urban locations in China, Korea, and Taiwan, PBM is dominantly found in fine particles ($PM_{2.5}$) and especially particles in the accumulation mode (0.1 – 2.0 μm diameter). A handful of studies reported the total mercury concentration in the particle size class with the highest concentration of PBM using units of pg m^{-3} of PBM per μg m^{-3} aerosol = pg μg^{-1} (Table 2). These studies report low mean PBM concentrations in cleaner coastal suburban areas of Taiwan (Fang et al., 2010), higher values in the more urban areas of Taiwan and Korea (Chen et al., 2012; Kim et al., 2012), and by far the highest values (up to 32 pg μg^{-1}) in the heavily polluted air of Shanghai (Chen et al., 2016; Xiu et al., 2009). In Shanghai, PBM concentrations as a function of particle size were determined on haze and non-haze days, where it was found that when the haze pollution was more severe the concentrations of PBM were higher, which suggested to the authors that the complex atmospheric conditions of haze days contributed to the growth of PBM in particles (Chen et al., 2016). In another study in Shanghai, a PBM maximum occurred in the accumulation mode, and a smaller secondary peak was observed in coarse mode particles (3-6 μm) (Chen et al., 2016). The authors suggest that the bimodal distribution demonstrated that PBM might have different formation mechanisms, including direct emissions from anthropogenic or natural sources and through the adsorption of gaseous mercury on mainly coarse particles. Furthermore, in Shanghai, the dominant size for PBM in the fine modes shifted from 0.32-0.56 μm during non-haze days to 0.56-1.0 μm during haze days, which revealed the higher growth velocity of PBM on haze-days due to the condensation and accumulation of mercury in particles (Chen et al., 2016). Keeler et al. (1995) observed a similar bimodal distribution of PBM in urban Detroit, Michigan.

At locations further downwind of major PBM sources and in coastal areas, PBM is more abundant on larger particles compared to what has been observed in large cities in Asia. Fang et al. (2010) observed

maximum PBM in the 2.5-10 μm size fraction in coastal Taiwan, similar to Feddersen et al. (2012) who found that the 3.3-4.7 μm size fraction had the most PBM in the coastal northeastern United States, and Wang et al. (2019) who found a tri-modal distribution in the South China Sea. PBM on coarse particles could be sea salt aerosols, which readily take up Hg^{II} (Wang et al. (2019); Section 2.4.2). Siudek et al. (2016) also found particles > 2.2 μm had the most PBM in Central Poland, and Fang et al. (2019) found the most PBM in the coarse mode at a polluted site in Taiwan. This presents an issue for the measurement of PBM, since a common instrument used for total PBM is the Tekran 1135, and the inlet of this instrument excludes particles larger than 2.5 μm, thereby potentially underestimating total PBM. This instrument is subject to additional biases, as described in Section 5.

2.6. Clouds and Fog

While it is well known that Hg^{II} can be absorbed by cloud and fog droplets (Section 2.3), understanding of the atmospheric chemistry of speciated mercury in clouds and fog is an emerging area of research. Both fog and clouds are a visible aggregation of liquid aerosols that are held aloft due to the turbulent movement of air (Roman et al., 2013). Fog is cloud in contact with the Earth's surface. Due to the relatively small size of fog and cloud droplets, they have a large surface area and promote scavenging of water-soluble gases and impaction of dry aerosol particles, which can lead to an enrichment of pollutants in fog and clouds (Degefie et al., 2015; Malcolm et al., 2003). Deposition via impaction of droplets with surfaces such as trees, plants, and human structures is known to be a major source of pollutants to many watersheds (Malcolm et al., 2003). Hg^0 can be oxidized, and Hg^{2+} can be reduced (Lin and Pehkonen, 1998), and inorganic mercury can be methylated (Li et al., 2018; Yin et al., 2012), in clouds and fog. Current research in this area has focused on 1) the degree of enrichment of total mercury and CH_3Hg^+ in clouds and fog and the identification of sources, 2) the potential for chemical processing within clouds and fog that affects mercury concentrations and speciation, and 3) the

mechanisms and thermodynamics of aqueous-phase chemistry that transform mercury species within the droplets.

We present a summary of measurements of total mercury and CH_3Hg^+ in cloud and fog water in Table 3, since these data, to our knowledge, have not been summarized before. The environments studied include marine stratus clouds over the open ocean, coastal fog, inland valley fog, and mountain-top clouds. Total mercury mean concentrations in cloud and fog water ranged from 9.2 ng L^{-1} in a marine stratus environment over the open ocean (Weiss-Penzias et al., 2018) to 70.5 ng L^{-1} in mountain-top cloud water downwind of an industrial area in China (Li et al., 2018). Intermediate concentration values of total mercury (~25 ng L^{-1}) were found in mountain top clouds far downwind of anthropogenic sources in northeastern North America (Malcom et al., 2003) and Taiwan (Sheu and Lin, 2011), as well as in marine fog water sampled in California (Weiss-Penzias et al., 2016a) and New Brunswick, Canada (Ritchie et al., 2006). At the relatively polluted site of Mount Tai, China, the arsenic concentration (a tracer of coal combustion) in cloud water was three times higher than in cloud water at a polluted site in eastern North America and 20 times higher than in cloud water over the open ocean (Li et al., 2018). Sulfate (also a coal-combustion tracer) concentrations in cloud water at Mount Tai were also elevated compared to other sites.

In contrast, CH_3Hg^+ mean concentrations were highest in coastal fog and clouds over the coastal ocean (0.87-1.6 ng L^{-1}), compared to that found in inland clouds and fog (0.2-0.5 ng L^{-1}). Recent evidence in coastal California has found that coastal marine clouds and fog absorb oceanic emissions of $(CH_3)_2Hg$ and CH_3Hg^+ and can act as a vector of CH_3Hg^+ to coastal terrestrial ecosystems (Weiss-Penzias et al., 2016a; Weiss-Penzias et al., 2018). This phenomenon may be restricted to the near coastline since CH_3Hg^+ concentrations at a site within 50 m of the ocean were 3.7 times higher than at a site 40 km

inland, indicating the potential for photodemethylation of CH_3Hg^+ during the advection of fog water from ocean to land (Weiss-Penzias et al., 2016a).

Table 3: Speciated mercury measurements (mean ± std. dev.) in clouds and fog. Mean As SO_4^{2-} concentrations for select studies are also shown as an indicator of coal combustion influence. Percents in the particle phase were determined via filtration (pore size ~0.5 μm).

Sample Type	Location	Dates	Total mercury (ng L^{-1})	Total CH_3Hg^+ (ng L^{-1})	% of total mercury in particle phase	% of CH_3Hg^+ in particle phase	As (μg L^{-1})	SO_4^{2-} (mg L^{-1})	Reference
Marine stratus cloud water	Coastal California	Summer, 2016	9.18 ± 5.98	0.87 ± 0.66			0.12	2.95	Weiss-Penzias et al. (2018)
Advective marine fog water	Coastal California	Summers, 2014, 2015	27.6 ± 25.8	1.6 ± 1.9	74%	94%		21.3	Weiss-Penzias et al. (2016a)
Valley radiation fog water	Inland California	Winter, 2016	24.0 ± 10.5	0.18 ± 0.09					Weiss-Penzias et al. (2018)
Valley radiation fog water	Inland California	Winter, 2003	11.0	0.5				31.1	Bittrich et al. (2011)
Mountain-top cloud water	Mountaintop New York	Summer 2010	4.3 ± 0.5	0.02 ± 0.00					Gerson et al. (2017)
Marine fog water	Bay of Fundy, Canada	Summer, 2003	2 to 435						Ritchie et al. (2006)
Mountain-top cloud water	Mountaintop Vermont	Summer-Fall, 1998	24.8				1.11	2.19	Malcolm et al. (2003)
Mountain-top cloud water	Mountaintop Taiwan	Winter, 2009	9.6					6.6	Sheu and Lin (2011)
Mountain-top cloud water	Mountaintop China	Summer, 2015	70.5 ± 100.6	0.15 ± 0.15	71%		5	39.0	Li et al. (2018)

The presence of CH_3Hg^+ in inland mountain-top and valley fogs and clouds far from the ocean suggests a CH_3Hg^+ formation mechanism must exist within the hydrometeors, with CH_3Hg^+ formation rates of sufficient magnitude to compensate for the continual loss of CH_3Hg^+ due to photodemethylation (Bittrich et al., 2011; Hammerschmidt et al., 2007; Li et al., 2018). Li et al. (2018) observed increased mass ratios of CH_3Hg^+ to dissolved total mercury in mountaintop cloud water in China that coincided

with decreased ionic strength. They suggested this could be an indicator of abiotic formation of CH_3Hg^+. The evidence suggests that higher ionic strength in cloud water inhibited methylation due to inorganic ions out-competing organic ligands that can potentially be methyl donors, such as acetate, methylcobalamin, methyl iodine, and other low-molecular-weight organics (Li et al., 2018). Furthermore, this study observed that CH_3Hg^+ in cloud water was significantly correlated with propionate, indicating formation of CH_3Hg^+ via alkylation by propionic acid as proposed by Yin et al. (2012). Future work is needed to identify methyl donors and methylation mechanisms.

Cloud water chemistry also affects the speciation of inorganic mercury compounds. Highly acidic (pH < 4) cloud water at Mount Bamboo displayed 10-20 times higher total mercury concentrations than cloud water at pH > 4 (Sheu and Lin, 2011). The authors suggest this is due to reduced oxidation of Hg^0 and/or enhanced Hg^{2+} reduction at higher pH values, a notion consistent with early studies (Lin and Pehkonen, 1999; Pleuel and Munthe, 1995). Some studies have shown GEM depletion during acidic fog events, which could mean that acidic fog can absorb and oxidize Hg^0 (Hall et al., 2006; Xiu et al., 2009)

Recent thermodynamic modeling work has focused on using stability constants (log K) of multiple chemical species of mercury including compounds with halides, sulfate, nitrate, nitrite, ammonia, carbonate, low-molecular-weight organics, and dissolved organic matter, to determine the dominant species of Hg^{2+} compounds present in cloud drops as a function of pH. Li et al. (2018) found that 50-90% of dissolved Hg^{2+} complexes with dissolved organic matter at pH < 6, whereas at pH > 6 the dissolved Hg^{2+} was found predominantly (> 60%) in the $Hg(OH)_2$ form. This finding was consistent with an earlier study that also found $Hg(OH)_2$ was the dominant form found in Sacramento Valley, California, where pH of fog water was on the basic side (5.7-6.8) (Bittrich et al., 2011). In the absence of dissolved organic matter, Bittrich et al. (2011) found that chloride complexes ($HgCl^+$ and $HgCl_2$) were the dominant chemical species of Hg^{2+}.

In summary, concentrations of total mercury and CH_3Hg^+ in cloud and fog water are generally enhanced above those typically found in rainwater due to 1) lower liquid water content in cloud and fog water, 2) greater rates of gas-particle scavenging due to smaller hydrometeor size, and 3) relatively increased acidity, which prevents the reduction of Hg^{2+} to Hg^0. Marine clouds and fog may become enriched in CH_3Hg^+ due to oceanic emissions of organic mercury compounds to the atmosphere and gas scavenging by acidic marine aerosols. CH_3Hg^+ in clouds and fog may also be produced in situ most likely due to an abiotic mechanism involving low-molecular-weight organic ligands that can donate a methyl group to Hg^{2+}.

3. Deposition

3.1. Wet Deposition

Sprovieri et al. (2010) reviewed worldwide atmospheric mercury measurements and included discussion of wet deposition. Sprovieri et al. (2017) found high spatial variability in wet deposition rates across the globe but demonstrated a general trend of highest wet deposition in the lower and mid-latitudes of the Northern Hemisphere, with lower deposition rates in the Arctic and the Southern Hemisphere. In North America, wet deposition tends to be highest in the southeastern United States (Prestbo and Gay, 2009; Weiss-Penzias et al., 2016b). Wet deposition in urban areas of China is higher than in North America and Europe (Fu et al., 2012b), but for rural areas, the values are similar (Fu et al., 2015). As with atmospheric mercury concentrations (Section 4.2), wet deposition amounts have decreased at many locations around the globe (Keeler et al., 2005; Muntean et al., 2014; Prestbo and Gay, 2009; Weiss-Penzias et al., 2016b; Zhang and Jaeglé, 2013).

Urban/industrial locations tend to have higher mercury wet deposition than rural/remote locations, but this association can be weak, because atmospheric processes, not just local emissions, are important

drivers of mercury uptake by precipitation (Sprovieri et al., 2010). Many studies have noted the influence of emission sources on spatial trends in mercury wet deposition (Fu et al., 2015; Gratz and Keeler, 2011; Gratz et al., 2013; Guo et al., 2008; Lynam et al., 2016; Ma et al., 2015; Michael et al., 2016; Qin et al., 2016; Siudek et al., 2016; Wang et al., 2014b; White et al., 2009), including at the global scale (Sprovieri et al., 2017). Weiss-Penzias et al. (2016b), Zhang et al. (2016), and a review by Obrist et al. (2018) showed that wet deposition follows temporal trends in global and regional anthropogenic mercury emissions.

Most studies report that wet mercury deposition is higher in warm seasons, and this has been attributed to more precipitation (Fu et al., 2015; Michael et al., 2016; Qin et al., 2016; Sanei et al., 2010; Seo et al., 2012; Sprovieri et al., 2017), more availability of Hg^{II} compounds in the atmosphere (Caffrey et al., 2010; Lynam et al., 2016), better efficiency of rain relative to snow at scavenging gas-phase Hg^{II} (Gratz et al., 2009; Landis et al., 2002; Selin and Jacob, 2008; White et al., 2013), or a higher prevalence of deep convective clouds (Lynam et al., 2016). While short rain events tend to lead to higher mercury concentrations in rainwater, annual wet deposition fluxes tend to be positively correlated with annual rainfall (Prestbo and Gay, 2009; Sprovieri et al., 2017).

Some researchers have shown significant positive correlations between total mercury concentrations in rainwater and mercury concentrations in surface-level ambient air (Brunke et al., 2016; Fu et al., 2015; Seo et al., 2012; Zhou et al., 2018a), while others have not (Mao et al., 2017b). Cheng and Zhang (2016) showed that relationships between atmospheric GOM and wet deposition are more reasonable when the known low bias in GOM measurements (Bu et al., 2018; Lyman et al., 2010; McClure et al., 2014) is taken into account.

Scavenging rates of surface-level GOM are higher in rain than in snow, while particle-phase mercury shows the opposite trend (Amos et al., 2012; Cheng et al., 2015; Lombard et al., 2011; Mao et al., 2012;

Seo et al., 2012; Zhou et al., 2018a). GOM scavenging tends to be dominant for both precipitation types, however (Seo et al., 2012; Zhou et al., 2018a), and a variety of studies confirm that GOM scavenging is, in general, more important than particulate scavenging for wet deposition (Bullock et al., 2009; Cheng et al., 2015; Sakata and Asakura, 2007; Selin and Jacob, 2008). Cheng et al. (2015) found that fine-particulate PBM and coarse-particulate PBM contributed 8–36% and 5–27%, respectively, depending on the location, to total wet deposition at nine wet deposition monitoring sites in North America. They estimated that gaseous Hg^{II} compounds contribute 39–87% to wet deposition. Amos et al. (2012) showed that model simulations with gas-particle partitioning better predicted wet deposition than simulations that did not include partitioning behavior.

Several recent papers highlight the influence on wet deposition of deep convective clouds that scavenge Hg^{II} from the middle and upper troposphere (Holmes et al., 2016; Kaulfus et al., 2017; Selin and Jacob, 2008; Shah and Jaeglé, 2017; Sprovieri et al., 2017). Emphasis has been placed on this phenomenon in the Gulf of Mexico region (Guentzel et al., 2001; Shanley et al., 2015; Sprovieri et al., 2017), but others have shown the importance of upper-atmosphere Hg^{II} scavenging on wet deposition in high-elevation areas (Gerson et al., 2017; Huang and Gustin, 2012; Kaulfus et al., 2017), and throughout the atmosphere generally (Holmes et al., 2016; Selin and Jacob, 2008). Change to the oxidation capacity of the atmosphere would affect mercury wet deposition. This is discussed in Section 4.2.4.

3.2. Dry Deposition

Measurement and modeling approaches for quantifying dry deposition of GOM and PBM and air-surface exchange fluxes of GEM, and field studies measuring GOM and PBM dry deposition and mercury in litterfall and throughfall were reviewed in detail by Wright et al. (2016). Measurement and modeling studies of air-surface exchange of GEM were also reviewed by Zhu et al. (2016). Dry deposition velocities

generated from field measurements were previously documented in Zhang et al. (2009). Future research needs were recommended in Zhang et al. (2017a). A summary of the major findings from earlier reviews, as well as recent progress in measurement and modeling studies of dry mercury deposition, are presented below. Measurement methods for dry mercury deposition are reviewed in Section 5.2.3. Change to the oxidation capacity of the atmosphere would affect mercury dry deposition. This is discussed in Section 4.2.4.

3.2.1. Measurement and Modeling Data

Field measurement data reviewed by Wright et al. (2016) showed that median values of GOM plus PBM dry deposition were on the order of ~10 μg m^{-2} yr^{-1} in Asia and ~6 μg m^{-2} yr^{-1} in North America. The difference between the two continents can be explained by the much higher anthropogenic emissions and thus ambient concentrations in Asia. The ranges of the values were similar between the two continents, e.g., from ~1.0 to 500 μg m^{-2} yr^{-1}. Few measurements of GOM and PBM dry deposition have been made in other parts of the world.

Modeled GOM plus PBM dry deposition fluxes (using methods that rely on measured air concentrations) tend to be in the same range as measurement values (though ambient air measurements of Hg^{II} are biased low; see Section 5). Modeled GOM plus PBM dry deposition data from Asia, Europe, and North America ranged from <0.1 to ~400 μg m^{-2} yr^{-1} (Wright et al., 2016). Median and mean modeled deposition were ten times higher in Asia than in Europe and North America, partly due to the higher ambient concentrations of GOM plus PBM in Asia. In a later study by Wright et al. (2016), multi-year averages of modeled GOM plus PBM dry deposition fluxes across North America were on the order of <1- 6 μg m^{-2} yr^{-1} with the exception of a high elevation site, where annual dry deposition was estimated to be ~60 μg m^{-2} yr^{-1}. GOM generally contributes more to dry deposition than PBM due to the faster deposition process of GOM.

Measurements of GEM fluxes have frequently shown bi-directional exchange features. Similar to GOM and PBM flux measurements, GEM flux data have mostly been obtained in East Asia and North America, while some data have been collected in Europe and little is available in other parts of the world. Most studies have focused on quantifying GEM emissions, rather than deposition because the amount of mercury emitted from natural surfaces has been estimated to be twice as much of the anthropogenic emissions globally (Zhu et al., 2016). GEM emission fluxes observed in East Asia are higher than those observed in the other continents, likely due to the re-emission of previously deposited mercury from anthropogenic sources (Zhu et al., 2016).

However, more recent studies have shown that Hg^0 dry deposition may be more important than previously assumed in earlier studies (Enrico et al., 2016; Obrist et al., 2017; Wright et al., 2016). Jiskra et al. (2018) hypothesize that one possible reason for this is that mercury deposited as Hg^{II} to leaf surfaces is more likely to re-emit than Hg^0 deposited through stomata (though Hg^0 has been shown to be sorbed to leaves via non-stomatal pathways as well; See Arnold et al. (2018) and Stamenkovic and Gustin (2009)). Net GEM dry deposition over vegetated canopies becomes increasingly important in regions where mercury input to soil from atmospheric dry and wet deposition of Hg^{II} is low, and thus mercury emissions from the soil are low. For example, a mass balance study supported by mercury stable isotope composition measurements revealed that atmospheric mercury deposition to a peat bog system was dominated by GEM dry deposition (Enrico et al., 2016). Another mass balance study coupled with comprehensive measurements of mercury stable isotopic signatures in all related media revealed that higher mercury content in Arctic soil compared to temperate soil was predominantly due to tundra uptake of GEM (Obrist et al., 2017). Modeling estimates of the dry deposition budget across North America confirmed that Hg^0 dry deposition to forest canopies is more important than dry deposition of GOM plus PBM on an annual basis, and this finding is supported by regional litterfall mercury data collected across eastern North America (Wright et al., 2016).

The number of available measurements of mercury in litterfall and throughfall has been increasing. Mercury content in litterfall and throughfall are generally higher in urban regions of Asia, followed by remote regions in Asia, then locations in Europe and North America (Wright et al., 2016). Mercury dry deposition was estimated by Wright et al. (2016) from concurrent measurements of litterfall, throughfall, and open-space wet deposition for forests with such data. They found that dry and wet deposition were equally important in the total deposition budget. A comparison of multi-year data of litterfall and wet deposition across the eastern and mid-western United States also suggests the same conclusion (Risch and Kenski, 2018).

Considering the importance of litterfall mercury in the dry deposition budget, global mercury deposition through litterfall was estimated based on the published litterfall mercury data and forest coverage worldwide (Wang et al., 2016). A total of ~1200 Mg yr^{-1} of litterfall mercury was obtained globally, which was several times higher than the estimated mercury emissions from forest landscapes. Since litterfall mercury is derived primarily from Hg^0 uptake through stomata (Zhang et al., 2012a), this suggests that global forest ecosystems are a strong sink for Hg^0.

3.2.2. Emerging Research Activities

The ultimate goal of quantifying atmospheric mercury deposition to various ecosystems is to assess the impact of mercury sources to human, animal, and ecosystem health (Wright et al., 2018). Thus, monitoring programs should be designed to better link the sources, transportation, and fates of atmospheric mercury by concurrently measuring mercury in all the concerned biological media. This has been done in a few recent studies. In a southwest China watershed, litterfall, throughfall, runoff, and soil concentrations of total mercury and CH_3Hg^+ were sampled for two years (Du et al., 2018), results from which showed litterfall as the predominant route for both total mercury and CH_3Hg^+ to the soil. The same study also found that total mercury and CH_3Hg^+ were concentrated in different media during

litter decomposition. Also, while a portion of wet-deposited mercury may be lost from the canopy floor through rainwater runoff, the majority of litterfall mercury is likely to remain on the forest floor for a long period. Thus, mercury dynamics in the process of litter decomposition is crucial to understanding the final fate of the dry deposited mercury and its input to soil and downstream aquatic systems in forest catchments. For example, Zhou et al. (2018b) measured mercury biogeochemical cycling and fractionation processes in coniferous and broadleaf forests in southwest China by measuring total mercury, CH_3Hg^+, and litterfall biomass in the process of litter decomposition over one year.

4. Spatial and Temporal Distribution

4.1. Spatial Patterns

An extensive review of GEM and GOM measurements over oceans and land was conducted by Mao et al. (2016). Thus, this section provides only a brief overview of the spatial distribution of atmospheric mercury. Uncertainty exists about the amount of Hg^{II} collected in GEM measurements, and most GOM measurements are known to be biased low (Section 5), so some of the information presented is likely only qualitative.

4.1.1. Marine Environments

Mao et al. (2016) analyzed 50+ measurement campaigns undertaken from 1965 to 2012. Average concentrations of GEM over the Pacific and Mediterranean Seas were higher than other marine environments. GEM over the Pacific was elevated due to mercury emissions outflow from Eastern China. Over the Mediterranean Sea, industrial pollution from Europe, meteorological conditions conducive to evasion of GEM from surface water, and emissions from shipping ports contributed to elevated concentrations (Sprovieri et al., 2010). Arctic and Antarctic concentrations of GEM were lower

owing to the poles' remoteness from anthropogenic emissions and atmospheric mercury depletion events (Steffen et al., 2008).

GEM in the northern hemisphere marine atmosphere is higher than the southern hemisphere, due in part to greater anthropogenic emissions in the northern hemisphere (Mao et al., 2016; Slemr et al., 2011; Sprovieri et al., 2016; Sprovieri et al., 2010). However, Soerensen et al. (2012) reported that the hemispheric gradient has decreased, possibly because declining ocean mercury concentrations in the North Atlantic have significantly reduced GEM evasion in that region.

GOM measurements have covered the Atlantic, Indian, Pacific, Arctic, and Antarctic Oceans, and the Mediterranean. Concentrations can be extremely high (>1000 pg m^{-3}) at the poles (Mao et al., 2016) during springtime depletion events that cause rapid conversion of Hg^0 to Hg^{II} (Steffen et al., 2013). Arctic mercury depletion events were treated in detail by Steffen et al. (2008), Steffen et al. (2015), and Dastoor et al. (2015).

4.1.2. Terrestrial Environments

Measurements of GEM and GOM in terrestrial environments have been summarized in previous review papers (Mao et al., 2016; Sprovieri et al., 2010). The GOM measurements in these reviews were mostly collected with KCl denuder-based systems, which are biased low (see Section 5). Spatial patterns of GEM on a regional scale have been analyzed across Canada (Cole et al., 2014), the United States (Amos et al., 2012; Weiss-Penzias et al., 2016b), the United Kingdom (Brown et al., 2015), and China (Fu et al., 2015). The survey by Mao et al. (2016) considered 100+ measurement campaigns at continental sites worldwide that were conducted between 2003 and 2013. The review paper compared GEM and GOM concentrations by region and by site characteristics and discussed driving mechanisms for the variability in GEM and GOM. On a global scale, mean GEM concentrations are higher in Asia than in Europe, and

North America. Urban sites tend to have the highest GEM concentrations. Mean concentrations are similar among remote, rural and high elevation sites.

Sprovieri et al. (2016) presented spatial patterns in GEM from the Global Mercury Observation System network. The paper reported 2010-2015 GEM measurements at 27 sites comprising 17 northern hemisphere sites, five tropical region sites, and five southern hemisphere sites. Their work showed GEM concentrations decreasing with latitude. They showed that, during 2013-2014, mean GEM concentrations were ~1.5 ng m^{-3} in the northern hemisphere, ~1.2 ng m^{-3} in the tropics and ~0.9 ng m^{-3} in the southern hemisphere.

Mao et al. (2016) also reviewed +65 measurement campaigns of GOM that were undertaken between 2003 and 2013. Few measurements of GOM have been reported at continental sites in Europe and the Southern Hemisphere. Mean GOM concentrations were similar at continental sites in the United States and Asia. GOM concentrations at continental Canadian sites were lower than those in the United States and Asia. Maximum concentrations in GOM have reached a few hundred pg m^{-3} in Canada and thousands of pg m^{-3} in the United States and Asia. Mean GOM concentrations at urban and high elevation continental locations were both elevated compared to rural and remote continental sites.

4.1.3. Upper Troposphere and Lower Stratosphere

Vertical distributions of GEM and GOM have been reported from several aircraft measurement studies. In flights over the southern United States and the North American Arctic, GEM concentrations were constant from the surface to altitudes of 4-6 km (Brooks et al., 2014; Mao et al., 2010). In the free troposphere, GEM concentrations were slightly lower than those in the boundary layer (Mao et al., 2010; Weigelt et al., 2016). Results from transcontinental flights show that GEM concentrations in the

stratosphere can drop to 0.25-0.7 ng m^{-3} (Slemr et al., 2009; Slemr et al., 2018). Depletion of GEM in stratospheric air masses was also confirmed in a flight over North America (Lyman and Jaffe, 2012).

GOM concentrations, in contrast, tend to increase with altitude. Brooks et al. (2014) observed a maximum concentration of 120 pg m^{-3} at 2-4 km above sea level during the summertime over the southern United States. In upper tropospheric air and air influenced by the stratosphere, GOM concentrations can reach several hundreds of pg m^{-3} (Fain et al., 2009; Gratz et al., 2015a; Lyman and Jaffe, 2012; Shah et al., 2016; Swartzendruber et al., 2006).

4.2. Temporal Trends and Potential Driving Mechanisms

4.2.1. Elemental Mercury Concentrations

Long-term trends in GEM concentrations have been reported for many ground stations, such as in Mace Head, Ireland; Cape Point, South Africa; Seoul, Korea; Okinawa, Japan, and across North America and the United Kingdom. These studies examined trends in GEM from the 1990s to as recently as 2016 and show that GEM concentrations have decreased from the 1990s to 2005-2013 (Brown et al., 2015; Cole et al., 2014; Ebinghaus et al., 2011; Kim et al., 2016; Martin et al., 2017; Marumoto et al., 2019; Slemr et al., 2011; Weigelt et al., 2015; Weiss-Penzias et al., 2016b; Zhang et al., 2016). Slemr et al. (2011) estimated an annual decreasing trend of 1.4% and 2.7% per year in the northern and southern hemispheres from 1996 to 2009, respectively. GEM concentrations at Mace Head decreased by 1.3% per year from 1996 to 2013 (Weigelt et al., 2015; Zhang et al., 2016). In the United Kingdom, a decrease of 21% from 2003 to 2013 equates to ~1.9% per year decrease (Brown et al., 2015). At Canadian sites, GEM concentrations fell by 0.9% to 3.3% per year since the 1990s based on ten sites with 5 to 15 years of data (Cole et al., 2014). GEM declines in the Arctic were smaller, ranging from 0.6% to 0.9% per year (Chen et al., 2015; Cole et al., 2013; Cole and Steffen, 2010). Aside from ground stations, shipboard

measurements have indicated that GEM decreases of 2.5% per year from 1977 to 2009 over the North Atlantic (Soerensen et al., 2012). Navrátil et al. (2018) showed that mercury concentrations in tree rings in central and eastern Europe have decreased from 1975 to 2015. The decreasing trend in GEM estimated using tree ring concentrations as a proxy was similar in magnitude to the observed GEM trend at Mace Head (Navrátil et al., 2018).

Beginning in the early to mid-2000s, several studies have observed a more modest decrease in GEM and even a constant or increasing trend in some cases. In North America, GEM concentrations showed a flat or less negative trend from 2008 to 2013 (Weiss-Penzias et al., 2016b). Weigelt et al. (2015) found a decreasing trend in GEM at Mace Head from 1996 to 2009, but GEM decreased at a slower pace from 2010 to 2013. GEM in Seoul, Korea remained constant from 2004 to 2011 (Kim et al., 2016). Increasing trends were found at Cape Point, South Africa, and two sites in China during the 2007-2015 and 2002-2013 periods, respectively (Fu et al., 2015; Martin et al., 2017). Potential explanations for these temporal trends are discussed in the following sections.

4.2.2. Anthropogenic Emissions

Trends in GEM concentrations have not always been consistent with those of global anthropogenic emissions (Slemr et al., 2011); however, this comparison depends on the emissions inventory. From 1980 to 2000, global anthropogenic emissions were constant, according to Streets et al. (2017), whereas for a part of this period (1990 to ~2005) atmospheric GEM concentrations have decreased as mentioned above. In contrast, a global anthropogenic emissions inventory developed by Zhang et al. (2016) found a decrease in emissions by 0.5-1.4% per year from 1990 to 2010. Model simulations using this inventory reproduced the decreasing trends in GEM in North America and Europe from 1990 to 2010. This inventory accounted for several important changes in emissions: (1) decreased emissions from commercial products, (2) increased artisanal and small-scale gold mining emissions in developing

countries, and (3) decreased power plant emissions due to the installation of pollution control devices and subsequent changes in emissions speciation. The uncertainties in the emissions ranged from -33% to 60% in the study by Zhang et al. (2016), while a previous emissions inventory showed that the uncertainties in emissions vary by continent (27-50%) and source type (25% to a factor of 3) (Pacyna et al., 2010). Therefore, an accurate global anthropogenic emissions inventory is essential for interpreting trends in atmospheric concentrations and assessing the effectiveness of mercury pollution control policies. Comparison with regional or local emissions might be more suitable for explaining long-term concentration trends. Studies in the United Kingdom and northeastern United States found that regional and local reductions in anthropogenic emissions significantly contributed to long-term declines in GEM (Brown et al., 2015; Zhou et al., 2017a).

From 2000-2015, there was a slight increase in global anthropogenic emissions (Streets et al., 2017; Streets et al., 2019), which may have contributed to the slower decline or increasing trend in GEM after 2005. Streets et al. (2019) estimated that global anthropogenic emissions have increased by 1.8% per year from 2010 (2188 Mg) to 2015 (2380 Mg). Anthropogenic emissions declined in North America and most of Europe, but increased in Central America, South Asia, and Eastern Africa. The increase in global anthropogenic emissions is attributed to caustic soda and cement production and artisanal gold mining in developing countries. The largest emissions in 2015 are from East Asia (Streets et al., 2019). However, annual anthropogenic emissions in China have stabilized from 2006 to 2014 (Streets et al., 2019; Wu et al., 2016).

4.2.3. Natural Emissions, Re-emissions, and Sinks

Anthropogenic mercury emissions only make up approximately one-third of the total emissions to the atmosphere (Pacyna et al., 2016; Slemr et al., 2011). Thus, changes in GEM might not be entirely due to changes in anthropogenic emissions. Natural emissions and re-emissions comprise 70% of the total

atmospheric emissions, and 36% of this is from oceans (Pacyna et al., 2016). Soerensen et al. (2012) observed a decrease in GEM of 2.5% per year over the North Atlantic from 1977 to 2010 and suggested that the decline was attributed to decreasing mercury concentrations in the ocean (80% decrease since 1980), which reduced evasion of GEM from the ocean. They found this process to be a more important factor contributing to the decrease in GEM than anthropogenic emissions reductions in North America and Europe. Possible reasons for the decrease in oceanic mercury include lower Hg^{II} deposition owing to decreasing Hg^{II} emissions, and a reduction in mercury effluent released to rivers (Soerensen et al., 2012).

On the other hand, the Arctic has experienced the opposite effect, according to Chen et al. (2015). Model simulations showed that rising temperatures in the last decade led to fewer depletion events and subsequently lower Hg^{II} deposition. The increasing temperatures also reduced the amount of sea ice, which enhanced GEM evasion. The combination of these factors led to a much weaker decreasing trend in GEM over the Arctic from 2000 to 2009 compared to those of North America and Europe (Chen et al., 2015). The increasing trend in GEM at Cape Point, South Africa from 2007 to 2015 has been attributed to biomass burning in the southern hemisphere and the ENSO (El-Niño Southern Oscillation) cycle (Martin et al., 2017). An increase in deposition via vegetation uptake of GEM could also explain the decrease in GEM concentrations since 1990, according to Jiskra et al. (2018). They noted that net primary production has been increasing since 1990, and that spatial patterns and seasonal variations in net primary production and CO_2 mixing ratios are consistent with those of GEM concentrations (Jiskra et al., 2018).

4.2.4. Oxidative capacity

Changes in atmospheric oxidant concentrations have the potential to affect long-term trends in Hg^0. As discussed in Section 2, important Hg^0 oxidants are thought to include Br, O_3, OH, and perhaps others

(H_2O_2, NO_3, etc.). We provide an overview of trends in atmospheric oxidants to assess their roles in affecting long-term trends in Hg^0. Most studies on the oxidative capacity of the atmosphere have focused on O_3, H_2O_2, OH, and nitrate radical.

In general, the global trend in tropospheric O_3 from the preindustrial era to ~2000 is positive (Alexander and Mickley, 2015; Chan and Vet, 2010; Hartmann et al., 2013; Murray et al., 2014), with one study suggesting a 24 ± 11% increase since the preindustrial era. Global background O_3 has continued to increase recently, though trends can vary by season (Chan and Vet, 2010; Cooper et al., 2012; Zhang and Jaffe, 2017), and in some areas of Europe and the eastern United States, O_3 has decreased due to regional reductions in precursor emissions (Simon et al., 2014; Yan et al., 2018). A comparison of 16 models suggests an increasing trend for OH of 7.0 ± 4.3% from preindustrial times to the present (Murray et al., 2014). Long-term variability in OH can be largely explained by tropospheric mean O_3 photolysis rates, water vapor, and emissions of NO_x and reactive carbon (Alexander and Mickley, 2015; Murray et al., 2014). Global mean OH is projected to increase (Gratz et al., 2015b) by 4-13% by 2050 due to increased water vapor and NO_x emissions from lightning, although the increase may be attenuated by increases in methane (Alexander and Mickley, 2015). Investigators have used ice core measurements to infer a 50-60% increase in atmospheric H_2O_2 over the past 100-200 years, with the largest increases observed after 1970 (Alexander and Mickley, 2015). Models suggest H_2O_2 and nitrate radicals have increased in the present day compared to preindustrial times by 18% and 130%, respectively (Murray et al., 2014). H_2O_2 trends in the future are expected to track OH radicals, while trends in nitrate radicals will likely depend on those of NO_x emissions (Alexander and Mickley, 2015). Knowledge of trends in atmospheric halogens is very limited. We are not aware of any information on the trends in atmospheric bromine. Cuevas et al. (2018) reported a factor of 3 increase in atmospheric iodine from 1950 to 2010 based on ice core measurements in the North Atlantic.

Overall, studies point to an increase in the oxidative capacity over the last century, and especially over the past several decades, which may have decreased Hg^0 concentrations in the atmosphere. Since these trends are expected to continue, continued decreases in Hg^0 can also be expected. Information is needed about trends in atmospheric Br. Improved understanding of Hg^0 oxidation mechanisms and kinetics (Section 2.1) would improve understanding of these phenomena.

5. Measurement Methods

Pandey et al. (2011) and Gustin et al. (2015) reviewed atmospheric mercury measurement methods and instrumentation. Both included comprehensive reviews of common and newly-developed measurement techniques. Pandey et al. discussed quality control and calibration considerations for GEM, and Gustin et al. detailed the challenges with GOM measurements. Reviews by Huang et al. (2014) and McLagan et al. (2016) focused specifically on passive methods for measurement of atmospheric mercury concentrations. Wright et al. (2016) reviewed dry deposition, litterfall, and throughfall methods. Zhang et al. (2017a) discussed problems with current measurement methods and made recommendations for improvements.

5.1. Monitoring Networks

Stylo et al. (2016) reviewed current atmospheric mercury monitoring networks. Major networks include the Global Mercury Observation System, the National Atmospheric Deposition Program's Atmospheric Mercury Network (mostly in North America), the Asia-Pacific Mercury Monitoring Network, and the Arctic Monitoring and Assessment Programme. Canada, the United Kingdom, Japan, Korea, and Australia also operate atmospheric monitoring networks. Mercury wet deposition networks are operated by the National Atmospheric Deposition Program (North America) and the Global Mercury Observation System. Recommendations from a number of papers (Kumari et al., 2015; Sprovieri et al.,

2016; Sprovieri et al., 2010; Stylo et al., 2016; Zhang et al., 2017a) and the Global Mercury Assessment 2018 (UNEP, 2019) find that the spatial coverage of atmospheric mercury measurements is inadequate, particularly in Latin America, the Caribbean, the Middle East, Africa, Russia, southern Asia, and the southern hemisphere. Stylo et al. (2016) noted that locations with higher and increasing anthropogenic mercury emissions, such as in Asia and South America, have relatively few atmospheric mercury monitoring sites. GEM is the routinely monitored form of atmospheric mercury, whereas there are fewer measurements of GOM and a scarcity of size-fractionated PBM measurements (Mao et al., 2016; Sprovieri et al., 2010). As has been highlighted in previous reviews (Fu et al., 2015; Zhang et al., 2017a), consistent data management practices, such as standard operating procedures, quality control checks and access to data, between monitoring networks are needed to ensure that all collected data are intercomparable.

5.2. Current Measurement Methods

5.2.1. Elemental Mercury

The vast majority of recent studies that have measured GEM (without speciation) have used pre-concentration on gold traps followed by thermal desorption into a cold-vapor atomic fluorescence detector. Most have used a Tekran 2537 analyzer (Agnan et al., 2018; Denzler et al., 2017; Hoglind et al., 2018; Howard and Edwards, 2018; Howard et al., 2017; Kamp et al., 2018; Karthik et al., 2017; Liu et al., 2017; Mao et al., 2017a; Martin et al., 2017; Mason et al., 2017; Nerentorp Mastromonaco et al., 2017; Obrist et al., 2017; Prete et al., 2018; Read et al., 2017; Sizmur et al., 2017; Spolaor et al., 2018; Yin et al., 2018; Yu et al., 2018; Zhang et al., 2017a). In some studies, samples were collected manually on gold traps followed by quantification by atomic fluorescence (Black et al., 2018; Wang et al., 2017; Zhou et al., 2017b) or atomic absorption (El-Feky et al., 2018), while a few recent studies used a Lumex

Zeeman atomic absorption analyzer (Kalinchuk et al., 2018a; Kalinchuk et al., 2018b), a Gardis-5 analyzer (Albuquerque et al., 2017), a laser-induced fluorescence system (Hynes et al., 2017a; Hynes et al., 2017b), and a mercury lidar system (Lian et al., 2018).

In spite of work that has been undertaken to determine whether Tekran 2537 or similar analyzers measure total gas-phase mercury or Hg^0, uncertainty still exists, as discussed by Gustin et al. (2015). A viable approach for measurement of total mercury is to employ a pyrolyzer that has been tested and shown to reduce most or all Hg^{II} compounds (e.g., see supplemental information for Lyman and Jaffe (2012) and supplemental information for Ambrose et al. (2015)) upstream of mercury analyzers. Quantitative exclusion of PBM from total mercury measurements with impactors or filters upstream of pyrolyzers is likely impossible, since impactors and filters likely either retain some GOM (Feng et al., 2000) or release PBM as GOM (Lynam and Keeler, 2002; Lynam and Keeler, 2005; Rutter et al., 2008; Rutter and Schauer, 2007a), depending on conditions. See Sections 2.4 and 5.2.2 for more discussion of these phenomena. GOM capture devices upstream of the analyzer can ensure that GEM measurements sample only Hg^0. Section 5.3 provides references for several GOM capture devices.

5.2.2. Speciated Mercury

Many continue to use KCl denuder-based systems (especially the Tekran 1130/1135 speciation system) to measure GOM, in spite of overwhelming evidence that KCl denuders suffer from a low bias in ambient air (see reviews by Pandey et al. (2011), Gustin et al. (2015), and Zhang et al. (2017a) and recent evidence for bias presented by Cheng and Zhang (2016) and Bu et al. (2018)). It is possible that KCl denuders perform well in some environments, but this has yet to be demonstrated and remains speculative. Some recent studies have acknowledged the potential for bias in their measurements (Lin et al., 2019; Liu et al., 2019; Xu et al., 2017; Zhang et al., 2017b; Zhou et al., 2019; Zhou et al., 2018a), but the majority have not (Castagna et al., 2018; Duan et al., 2017b; Fang et al., 2018; Lin et al., 2019; Lin

et al., 2017; Shen et al., 2017; Tang et al., 2018). None of these studies incorporated GOM calibrations, as has been called for repeatedly (Gustin et al., 2015; Jaffe et al., 2014; Lyman et al., 2016; Pandey et al., 2011; Zhang et al., 2017a). Many KCl denuder-based and other atmospheric measurement studies indicated they followed operating procedures and quality assurance guidelines established by measurement networks, including the Global Mercury Observation System (Castagna et al., 2018; Howard et al., 2017; Karthik et al., 2017; Liu et al., 2019; Martin et al., 2017; Nerentorp Mastromonaco et al., 2017; Read et al., 2017; Spolaor et al., 2018) and the Atmospheric Mercury Network (Mao et al., 2017a).

Many recent studies utilized automated Tekran speciation systems to measure PBM (with aerodynamic diameter <2.5 μm), and these are mentioned above. Others used high-volume particle samplers, usually with quartz fiber filters that were baked before sampling to remove residual mercury (Albuquerque et al., 2017; Cheng et al., 2017; Duan et al., 2017a; Guo et al., 2017; Han et al., 2018; Li et al., 2017; Morton-Bermea et al., 2018; Qie et al., 2018; Yu et al., 2019). After sampling, filters were analyzed using a variety of standard methods. Several studies have shown that these traditional particle sampling methods lead to biases for particulate mercury. GOM can adhere to filter material or to collected particulate matter (Gustin et al., 2015; Pandey et al., 2011; Rutter and Schauer, 2007a; Talbot et al., 2011) and particulate mercury can re-volatilize and be lost from filters during collection (Gustin et al., 2015; Lynam and Keeler, 2002; Lynam and Keeler, 2005; Rutter et al., 2008), possibly via reduction of Hg^{II} compounds to Hg^0 (Malcolm and Keeler, 2007). Particulate-bound mercury measured by Tekran speciation systems has also been shown to suffer from bias (Gustin et al., 2015), and no particle-bound mercury measurements are calibrated (Gustin et al., 2015; Jaffe et al., 2014). Unfortunately, no particulate mercury measurement system has been demonstrated to be free from interferences and bias.

5.2.3. Dry Deposition

Most existing measurement methods for quantifying dry deposition and air-surface exchange fluxes of speciated atmospheric mercury can be grouped into three major categories, including micrometeorological approaches, dynamic gas flux chambers, and surrogate surface approaches (Wright et al., 2016; Zhu et al., 2016). Other methods (GEM/^{222}Rn ratio, GEM/CO ratio, enriched isotope tracer) have also been occasionally used (Zhu et al., 2016). Flux measurements using any of these approaches are subject to large uncertainties. For example, concentrations at different heights need to be measured using the micrometeorological approaches, but measuring mercury at low concentrations is challenging due to technological limitations of the available instruments (Jaffe et al., 2014). Dynamic gas flux chambers can be deployed over soil, water, low canopy, or tree branches, and have been used for GEM (Carpi et al., 2007; Eckley et al., 2011; Lyman et al., 2007) and GOM (Miller et al., 2019). The measured fluxes may not be representative of an entire area, however, due to heterogeneity in land use cover. Also, different designs inside the dynamic gas flux chambers can cause the measured fluxes to differ by up to one order of magnitude (Eckley et al., 2010). Surrogate surfaces may not perform the same way as natural surfaces in collecting mercury, and uncertainties in measured GOM and PBM dry deposition are larger than a factor of two depending on the selected surrogate surfaces and instrument setup (as detailed in Wright et al. (2016)). A new surrogate surface sampler was recently developed utilizing a three-dimensional deposition surface, which is expected to mimic the physical structure of many natural surfaces more closely than the traditional flat surrogate surface designs (Hall et al., 2017). Collocated measurements using different techniques should be performed to constrain measurement uncertainties (Fritsche et al., 2008; Osterwalder et al., 2018; Zhu et al., 2015). Standardized protocols should be developed for commonly used measurement techniques.

Measurements of mercury in litterfall and throughfall have been increasingly used to provide knowledge of mercury deposition over forest canopies. The majorify of mercury in litterfall is considered to be from stomatal uptake of Hg^0 (Zhang et al., 2012a) and can be used as a rough and conservative estimation of atmospheric mercury dry deposition (the portion that is retained in leaves). Mercury in throughfall also includes a portion of previously dry deposited mercury (the portion that is washed off from the canopy). Concurrent measurements of litterfall, throughfall, and open-space wet deposition measurements can be used to estimate dry deposition on seasonal or longer time scales, whereby dry deposition is approximated as litterfall plus throughfall minus open-space wet deposition (Wright et al., 2016).

Modeling methods for estimating mercury dry deposition either use the inferential approach, which calculates flux as the product of surface air concentration and modeled dry deposition velocity of speciated mercury (Engle et al., 2010; Gustin et al., 2012; Lyman et al., 2007; Marsik et al., 2007; Peterson et al., 2012; Zhang et al., 2012b), or use the bi-directional air-surface exchange model, which simulates emission from and deposition to land surfaces simultaneously (Baker and Bash, 2012; Xu et al., 1999). While the inferential approach has been used for GOM, PBM, and GEM, the bidirectional air-surface exchange approach is generally only used for GEM. Note that flux uncertainties in these modeling approaches are expected to be on a similar order of magnitude to those of field flux measurements because models were initially developed and validated using the limited flux measurements.

5.2.4. Wet Deposition and Cloud/Fog Water Mercury

Unlike methods for measurement of dry deposition, wet deposition measurement methods are well-established and have been standardized by measurement networks (Prestbo and Gay, 2009; Sprovieri et al., 2017). Various collectors have been used (Guentzel et al., 1995; Landis and Keeler, 1997; Morrison et al., 1995; Sakata and Marumoto, 2005), but all involve collection of precipitation through funnels and

into trace-cleaned bottles, usually with a cover that opens during rain events. Samples are then analyzed in the laboratory via standard protocols for total, methylated, and/or particulate-bound mercury.

Wet deposition samples have been collected over different timescales, impacting how data can be utilized. The National Atmospheric Deposition Program collects weekly samples (Prestbo and Gay, 2009), while the Global Mercury Observation System collects semi-weekly samples at most sites (Sprovieri et al., 2017). These sampling frequencies provide data that are useful for quantifying total deposition or understanding longer-term trends (Vijayaraghavan et al.; Weiss-Penzias et al., 2016b). In some studies, event-based samples, which can be used to understand short-term meteorological influences and source contributions, have been collected (Hoyer et al., 1995; Keeler et al., 2005; Landing et al., 2010; Marumoto and Matsuyama, 2014; White et al., 2013).

Cloud and fog water samples are collected by drawing droplet-laden air through Teflon strands and/or rods. Water adsorbs to the Teflon and runs down into a sample outlet, where it is collected in bottles (Demoz et al., 1996; Ritchie et al., 2006; Weiss-Penzias et al., 2012). Laboratory analysis methods for fog and cloud water samples are the same as for wet deposition.

5.3. New and Alternate Methods

McClure et al. (2014) and Gratz et al. (2019) installed a pyrolyzer upstream of a Tekran 2537 mercury analyzer when sampling the ambient atmosphere, providing clarity about the forms of mercury they measured (see discussion in the Introduction and Section 5.2.1). Some work has been done recently to improve Tekran 2537 detection by post-processing detector output (Ambrose, 2017). Srivastava and Hodges (2018) have developed a laser detection method that could be applied to ambient air, and they used that method to compare against established vapor pressure-temperature relationships. Their

measurements were within the range of uncertainty of those reported by Huber et al. (2006) and Quétel et al. (2016), but were 8.5% higher than those reported by Dumarey et al. (2010). Additional alternative collection methods have been developed and have potential for ambient air measurement, including gold nanoparticles followed by atomic fluorescence detection (Bearzotti et al., 2018) and nanofiber chemosensors (Macagnano et al., 2017a; Macagnano et al., 2017b).

A wide variety of passive samplers are in recent use or under development, with all but one (Fang et al., 2017) focusing on GEM. Studies used activated carbon (Lin et al., 2017; McLagan et al., 2018), gold nanoparticles (Papa et al., 2018; Santos et al., 2017), or other substrates (Fang et al., 2017; Lin et al., 2017; Macagnano et al., 2018) to collect mercury from ambient air.

Several new measurement methods for Hg^{II} have been developed recently. Slemr et al. (2018) reported aircraft measurements that used quartz wool traps for GOM (see also Lyman and Jaffe (2012)), though the authors acknowledge a potential for bias under some conditions (Ambrose et al., 2015; Ambrose et al., 2013; Hynes et al., 2017b). Cation-exchange membranes continue to be used to capture GOM (Huang and Gustin, 2015; Huang et al., 2015), and recent work has confirmed they perform better than KCl denuders (Bu et al., 2018) and do not absorb appreciable amounts of Hg^0 (Miller et al., 2019). A mercury speciation system that collects total mercury by passing air through a pyrolyzer and oxidized mercury by passing air through a cation-exchange membrane has been successfully deployed from aircraft (Ambrose et al., 2015; Gratz et al., 2015a). Cation-exchange membranes may be subject to bias in some conditions (Huang and Gustin, 2015). Additional information about membrane methods can be found in Section 2.1.5. Other Hg^{II} collection surfaces, including zirconia (Urba et al., 2017) and KCl-coated filters and sand (Bu et al., 2018), also show promise.

Marusczak et al. (2016) added mercury in the Tekran speciation system's flush cycle (flush of zero air before KCl denuder is heated) to mercury recovered from the denuder and found that this method led

to comparable results between KCl denuder measurements and measurements made with polyethersulfone membranes. The cation-exchange membranes mentioned in the previous paragraph are made of polyethersulfone, but they are also treated with a proprietary process that confers cation exchange properties. It is not known how these two membrane types compare with each other, or whether the use of flush data with denuder desorption data in Tekran speciation systems is an adequate method to correct biases in speciation system Hg^{II} results.

6. Key Uncertainties and Research Needs

6.1. Oxidation Mechanisms

Several sources of uncertainty around gas-phase mercury speciation and chemistry create a need for additional work. First, better constraints on reaction kinetics and associated rate constants are needed to more accurately inform the mechanisms deployed in chemical models. Consistent measurements of speciated mercury and improved spatiotemporal coverage of those measurements are also needed, especially since most previous measurements of GOM and PBM have been uncalibrated. This includes measurements across diverse ambient environments, vertically within the troposphere, and at different times of the year to capture the impact of meteorological and chemical conditions on speciated mercury concentrations.

Continued development of measurement techniques that avoid biases from other atmospheric constituents, and that can identify the chemical composition of GOM, is also needed. These improvements in measurement methods and spatiotemporal data coverage can more accurately inform chemical modeling efforts and, in turn, more clearly identify the oxidation mechanism(s) that govern ambient gaseous mercury chemistry.

6.2. Particle-phase Processes

While several studies have determined gas-particle partitioning relationships for Hg^{II}, these studies were based on uncalibrated measurements made with methods known to contain bias. While these studies likely capture the qualitative aspects of Hg^{II} gas-particle partitioning, calibrated, unbiased measurements of gas- and particle-phase Hg^{II} are needed to improve quantitative understanding of this phenomenon.

The relationship between aerosol particle size distribution and particle-bound Hg^{II} concentrations is an area of emerging research, especially in urban environments where particle loadings are high. Currently, little knowledge exists about the different formation mechanisms of particle-bound Hg^{II}, whether from direct emissions or through adsorption of gas-phase mercury on preexisting particles. A better understanding of the growth velocity of particle-bound Hg^{II} during haze days in megacities such as Shanghai is of the utmost importance, since PBM has been observed to be enriched in accumulation mode particles, and this size class is the most relevant in terms of human health effects.

6.3. Cloud Chemistry

Uncertainty exists regarding the aqueous chemistry of CH_3Hg^+ in cloud and fog droplets. There is currently no accepted mechanism of CH_3Hg^+ formation from inorganic mercury through an abiotic mechanism within a hydrometeor, and more work is needed in this area, both in the laboratory and the field. Also, additional measurements of CH_3Hg^+ in marine clouds and fog are needed to determine a possible source from oceanic emissions of CH_3HgCH_3. Measurements of CH_3Hg^+ in clouds, fog, and rain affected by urban emissions could help elucidate potential pathways of CH_3Hg^+ abiotic synthesis in polluted environments.

6.4. Dry Deposition

Stable isotope and flux studies have shown that Hg^0 dominates total dry deposition in some environments. Direct measurements of Hg^{II} deposition have been extremely few, however (surrogate surfaces, deposition models, and throughfall measurements do not directly detect Hg^{II} surface fluxes to natural surfaces). Direct flux measurements of Hg^{II} are needed, but may be impractical due to technological limitations. Alternatively, simultaneous quantification of Hg flux using multiple existing methods (GEM air-surface exchange, surrogate surfaces, litterfall, throughfall, inferential models) will likely better constrain method uncertainties than using any single method and may provide a more complete picture of mercury dry deposition/air-surface exchange processes.

6.5. Spatial and Temporal Trends

In the last ten years, GEM concentrations have decreased modestly in many areas, but have been increasing in some regions. Climates, emission sources, and atmospheric composition will continue to change, and continuation of globally-distributed long-term measurements is needed to track these trends, identify persistent and new sources of mercury, and assess the efficacy of mercury pollution control policies. The impact that climate change may have on the mercury biogeochemical cycle is at present highly speculative (Krabbenhoft and Sunderland, 2013; Obrist et al., 2018; Selin, 2014; Stern et al., 2012).

6.6. Measurement Techniques

Many atmospheric mercury measurements have been made with inadequate specificity and insufficient field validation. This is true for measurements that have targeted Hg^0 and those that have targeted gas- and particle-phase Hg^{II}. Future mercury measurements must use methods wherein the captured species

are clearly and quantitatively understood. Many emerging techniques and modifications of existing techniques appear able to meet this need. Future measurements must also be supported by routine calibration checks in ambient air in real field conditions. Field calibration techniques are readily available for Hg^0, are becoming available for gas-phase Hg^{II}, and are unavailable (to our knowledge) for particle-phase Hg^{II}.

7. Author Contributions

All authors contributed to all sections of this document. Seth Lyman edited the document and led the review effort. Lynne Gratz led the gas-phase chemistry section. Irene Cheng led the gas-particle partitioning and trends sections. Peter Weiss-Penzias led the particulate-bound mercury and cloud and fog sections. Leiming Zhang led the dry deposition section. Seth Lyman led the wet deposition and measurement methods sections. Except for the first author, author order was determined alphabetically.

8. Acknowledgements

The preparation of this manuscript was supported in part by U.S. National Science Foundation grant number 1700722.

9. References

Agnan Y, Douglas TA, Helmig D, Hueber J, Obrist D. Mercury in the Arctic tundra snowpack: temporal and spatial concentration patterns and trace gas exchanges. Cryosphere 2018; 12: 1939-1956.

Albuquerque M, Coutinho M, Rodrigues J, Ginja J, Borrego C. Long-term monitoring of trace metals in PM10 and total gaseous mercury in the atmosphere of Porto, Portugal. Atmos. Pollut. Res. 2017; 8: 535-544.

Alexander B, Mickley LJ. Paleo-Perspectives on Potential Future Changes in the Oxidative Capacity of the Atmosphere Due to Climate Change and Anthropogenic Emissions. Curr. Pollut. Rep. 2015; 1: 57-69.

Ambrose JL. Improved methods for signal processing in measurements of mercury by Tekran® 2537A and 2537B instruments. Atmos. Meas. Tech. 2017; 10: 5063-5073.

Ambrose JL, Gratz LE, Jaffe DA, Campos T, Flocke FM, Knapp DJ, Stechman DM, Stell M, Weinheimer AJ, Cantrell CA, Mauldin RL. Mercury emission ratios from coal-fired power plants in the Southeastern United States during NOMADSS. Environ. Sci. Technol. 2015; 49: 10389-10397.

Ambrose JL, Lyman SN, Huang J, Gustin MS, Jaffe DA. Fast time resolution oxidized mercury measurements during the Reno Atmospheric Mercury Intercomparison Experiment (RAMIX). Environ. Sci. Technol. 2013; 47: 7285-7294.

Amos HM, Jacob DJ, Holmes C, Fisher JA, Wang Q, Yantosca RM, Corbitt ES, Galarneau E, Rutter A, Gustin M, Steffen A, Schauer J, graydon JA, St. Louis VL, Talbot R, Edgerton E, Zhang Y, Sunderland EM. Gas-particle partitioning of atmospheric Hg (II) and its effect on global mercury deposition. Atmos. Chem. Phys. 2012; 12: 591-603.

Ariya PA, Amyot M, Dastoor A, Deeds D, Feinberg A, Kos G, Poulain A, Ryjkov A, Semeniuk K, Subir M. Mercury physicochemical and biogeochemical transformation in the atmosphere and at atmospheric interfaces: A review and future directions. Chem. Rev. 2015; 115: 3760-3802.

Arnold J, Gustin MS, Weisberg PJ. Evidence for nonstomatal uptake of Hg by aspen and translocation of Hg from foliage to tree rings in Austrian pine. Environ. Sci. Technol. 2018; 52: 1174-1182.

Baker KR, Bash JO. Regional scale photochemical model evaluation of total mercury wet deposition and speciated ambient mercury. Atmos. Environ. 2012; 49: 151-162.

Barrett JR. Rice is a significant source of methylmercury: research in china assesses exposures. Environ. Health Perspect. 2010: A398.

Bearzotti A, Papa P, Macagnano A, Zampetti E, Venditti I, Fioravanti R, Fontana L, Matassa R, Familiari G, Fratoddi I. Environmental Hg vapours adsorption and detection by using functionalized gold nanoparticles network. Journal of Environmental Chemical Engineering 2018; 6: 4706-4713.

Bernhoft RA. Mercury toxicity and treatment: a review of the literature. J. Environ. Public Health 2012; 2012.

Bittrich D, Rutter A, Hall B, Schauer J. Photodecomposition of methylmercury in atmospheric waters. Aerosol Air Qual. Res. 2011; 11: 290-298.

Black O, Chen J, Scircle A, Zhou Y, Cizdziel JV. Adaption and use of a quadcopter for targeted sampling of gaseous mercury in the atmosphere. Environ. Sci. Pollut. Res. 2018; 25: 13195-13202.

Brooks S, Ren X, Cohen M, Luke WT, Kelley P, Artz R, Hynes A, Landing W, Martos B. Airborne vertical profiling of mercury speciation near Tullahoma, TN, USA. Atmosphere 2014; 5: 557-574.

Brooks SB, Saiz-Lopez A, Skov H, Lindberg SE, Plane JM, Goodsite ME. The mass balance of mercury in the springtime arctic environment. Geophys. Res. Lett. 2006; 33: L13812.

Brown RJC, Goddard SL, Butterfield DM, Brown AS, Robins C, Mustoe CL, McGhee EA. Ten years of mercury measurement at urban and industrial air quality monitoring stations in the UK. Atmos. Environ. 2015; 109: 1-8.

Brunke E-G, Walters C, Mkololo T, Martin L, Labuschagne C, Silwana B, Slemr F, Weigelt A, Ebinghaus R, Somerset V. Mercury in the atmosphere and in rainwater at Cape Point, South Africa. Atmos. Environ. 2016; 125: 24-32.

Bu X, Zhang H, Lv G, Lin H, Chen L, Yin X, Shen G, Yuan W, Zhang W, Wang X, Tong Y. Comparison of Reactive Gaseous Mercury Collection by Different Sampling Methods in a Laboratory Test and Field Monitoring. Environ. Sci. Technol. Lett. 2018; 5: 600-607.

Bullock OR, Atkinson D, Braverman T, Civerolo K, Dastoor A, Davignon D, Ku JY, Lohman K, Myers TC, Park RJ, Seigneur C, Selin NE, Sistla G, Vijayaraghavan K. An analysis of simulated wet deposition of mercury from the North American Mercury Model Intercomparison Study. J. Geophys. Res. Atmos. 2009; 114: D08301.

Caffrey J, Landing W, Nolek S, Gosnell K, Bagui S, Bagui S. Atmospheric deposition of mercury and major ions to the Pensacola (Florida) watershed: spatial, seasonal, and inter-annual variability. Atmos. Chem. Phys. 2010; 10: 5425-5434.

Calvert JG, Lindberg SE. Mechanisms of mercury removal by O3 and OH in the atmosphere. Atmos. Environ. 2005; 39: 3355-3367.

Carlton AG, Turpin BJ. Particle partitioning potential of organic compounds is highest in the Eastern US and driven by anthropogenic water. Atmos. Chem. Phys. 2013; 13: 10203-10214.

Carpi A, Frei A, Cocris D, McCloskey R, Contreras E, Ferguson K. Analytical artifacts produced by a polycarbonate chamber compared to a Teflon chamber for measuring surface mercury fluxes. Anal. Bioanal. Chem. 2007; 388: 361-365.

Castagna J, Bencardino M, D'Amore F, Esposito G, Pirrone N, Sprovieri F. Atmospheric mercury species measurements across the Western Mediterranean region: Behaviour and variability during a 2015 research cruise campaign. Atmos. Environ. 2018; 173: 108-126.

Castro-González M, Méndez-Armenta M. Heavy metals: Implications associated to fish consumption. Environ. Toxicol. Pharmacol. 2008; 26: 263-271.

Chan E, Vet RJ. Baseline levels and trends of ground level ozone in Canada and the United States. Atmos. Chem. Phys. 2010; 10: 8629-8647.

Chen L, Zhang Y, Jacob DJ, Soerensen AL, Fisher JA, Horowitz HM, Corbitt ES, Wang X. A decline in Arctic Ocean mercury suggested by differences in decadal trends of atmospheric mercury between the Arctic and northern midlatitudes. Geophys. Res. Lett. 2015; 42: 6076-6083.

Chen S-J, Lo C-T, Fang G-C, Huang C-S. Particulate-bound mercury (Hg [p]) size distributions in central Taiwan. Environ. Forsensics 2012; 13: 98-104.

Chen X, Balasubramanian R, Zhu Q, Behera SN, Bo D, Huang X, Xie H, Cheng J. Characteristics of atmospheric particulate mercury in size-fractionated particles during haze days in Shanghai. Atmos. Environ. 2016; 131: 400-408.

Cheng I, Zhang L. Uncertainty assessment of gaseous oxidized mercury measurements collected by Atmospheric Mercury Network. Environ. Sci. Technol. 2016; 51: 855-862.

Cheng I, Zhang L, Blanchard P. Regression modeling of gas-particle partitioning of atmospheric oxidized mercury from temperature data. J. Geophys. Res. Atmos. 2014; 119: 11850-11863.

Cheng I, Zhang L, Mao H. Relative contributions of gaseous oxidized mercury and fine and coarse particle-bound mercury to mercury wet deposition at nine monitoring sites in North America. J. Geophys. Res. Atmos. 2015; 120: 8549-8562.

Cheng N, Duan L, Xiu G, Zhao M, Qian G. Comparison of atmospheric PM2.5-bounded mercury species and their correlation with bromine and iodine at coastal urban and island sites in the eastern China. Atmos. Res. 2017; 183: 17-25.

Ci Z, Zhang X, Wang Z, Niu Z. Atmospheric gaseous elemental mercury (GEM) over a coastal/rural site downwind of East China: temporal variation and long-range transport. Atmos. Environ. 2011; 45: 2480-2487.

Cohen MD, Draxler RR, Artz RS, Blanchard P, Gustin MS, Han Y-J, Holsen TM, Jaffe DA, Kelley P, Lei H, Loughner CP, Luke WT, Lyman SN, Niemi D, Pacyna JM, Pilote M, Poissant L, Ratte D, Ren X, Steenhuisen F, Steffen A, Tordon R, Wilson SJ. Modeling the global atmospheric transport and deposition of mercury to the Great Lakes. Elem. Sci. Anth. 2016; 3: 118.

Cole A, Steffen A, Pfaffhuber KA, Berg T, Pilote M, Poissant L, Tordon R, Hung H. Ten-year trends of atmospheric mercury in the high Arctic compared to Canadian sub-Arctic and mid-latitude sites. Atmos. Chem. Phys. 2013; 13: 1535-1545.

Cole AS, Steffen A. Trends in long-term gaseous mercury observations in the Arctic and effects of temperature and other atmospheric conditions. Atmos. Chem. Phys. 2010; 10: 4661-4672.

Cole AS, Steffen A, Eckley CS, Narayan J, Pilote M, Tordon R, Graydon JA, St. Louis VL, Xu X, Branfireun BA. A survey of mercury in air and precipitation across canada: Patterns and trends. Atmosphere 2014; 5: 635-668.

Cooper OR, Gao RS, Tarasick D, Leblanc T, Sweeney C. Long-term ozone trends at rural ozone monitoring sites across the United States, 1990-2010. J. Geophys. Res. Atmos. 2012; 117.

Cuevas CA, Maffezzoli N, Corella JP, Spolaor A, Vallelonga P, Kjær HA, Simonsen M, Winstrup M, Vinther B, Horvat C, Fernandez RP, Kinnison D, Lamarque JF, Barbante C, Saiz-Lopez A. Rapid increase in atmospheric iodine levels in the North Atlantic since the mid-20th century. Nat. Commun. 2018; 9.

Dastoor A, Ryzhkov A, Durnford D, Lehnherr I, Steffen A, Morrison H. Atmospheric mercury in the Canadian Arctic. Part II: Insight from modeling. Sci. Total Environ. 2015; 509: 16-27.

de Foy B, Tong Y, Yin X, Zhang W, Kang S, Zhang Q, Zhang G, Wang X, Schauer JJ. First field-based atmospheric observation of the reduction of reactive mercury driven by sunlight. Atmos. Environ. 2016; 134: 27-39.

De Simone F, Artaxo P, Bencardino M, Cinnirella S, Carbone F, D'Amore F, Dommergue A, Feng XB, Gencarelli CN, Hedgecock IM. Particulate-phase mercury emissions from biomass burning and impact on resulting deposition: a modelling assessment. Atmos. Chem. Phys. 2017; 17: 1881-1899.

De Simone F, Gencarelli CN, Hedgecock IM, Pirrone N. Global atmospheric cycle of mercury: A model study on the impact of oxidation mechanisms. Environ. Sci. Pollut. Res. 2014; 21: 4110-4123.

Deeds DA, Ghoshdastidar A, Raofie F, Guérette El-Ae, Tessier A, Ariya PA. Development of a Particle-Trap Preconcentration-Soft Ionization Mass Spectrometric Technique for the Quantification of Mercury Halides in Air. Anal. Chem. 2015; 87: 5109-5116.

Degefie D, El-Madany T-S, Held M, Hejkal J, Hammer E, Dupont J-C, Haeffelin M, Fleischer E, Klemm O. Fog chemical composition and its feedback to fog water fluxes, water vapor fluxes, and microphysical evolution of two events near Paris. Atmos. Res. 2015; 164: 328-338.

Demoz B, Collett Jr J, Daube Jr B. On the Caltech active strand cloudwater collectors. Atmos. Res. 1996; 41: 47-62.

Denzler B, Bogdal C, Henne S, Obrist D, Steinbacher M, Hungerbühler K. Inversion Approach to Validate Mercury Emissions Based on Background Air Monitoring at the High Altitude Research Station Jungfraujoch (3580 m). Environ. Sci. Technol. 2017; 51: 2846-2853.

Dibble T, Zelie M, Mao H. Thermodynamics of reactions of ClHg and BrHg radicals with atmospherically abundant free radicals. Atmos. Chem. Phys. 2012; 12: 10271-10279.

Dibble TS, Schwid AC. Thermodynamics limits the reactivity of BrHg radical with volatile organic compounds. Chem. Phys. Lett. 2016; 659: 289-294.

Driscoll CT, Mason RP, Chan HM, Jacob DJ, Pirrone N. Mercury as a global pollutant: sources, pathways, and effects. Environ. Sci. Technol. 2013; 47: 4967-4983.

Du H, Ma M, Sun T, An S, Igarashi Y, Wang D. Methyl and total mercury in different media and associated fluxes in a watershed forest, Southwest China. Int. J. Environ. Res. Public Health 2018; 15.

Duan L, Cheng N, Xiu G, Wang F, Chen Y. Characteristics and source appointment of atmospheric particulate mercury over East China Sea: Implication on the deposition of atmospheric particulate mercury in marine environment. Environ. Pollut. 2017a; 224: 26-34.

Duan L, Wang X, Wang D, Duan Y, Cheng N, Xiu G. Atmospheric mercury speciation in Shanghai, China. Sci. Total Environ. 2017b; 578: 460-468.

Dumarey R, Brown RJ, Corns WT, Brown AS, Stockwell PB. Elemental mercury vapour in air: the origins and validation of the 'Dumarey equation'describing the mass concentration at saturation. Accredit. Qual. Assur. 2010; 15: 409-414.

Durnford D, Dastoor A. The behavior of mercury in the cryosphere: A review of what we know from observations. J. Geophys. Res. Atmos. 2011; 116.

Ebinghaus R, Banic C, Beauchamp S, Jaffe D, Kock HH, Pirrone N, Poissant L, Sprovieri F, Weiss-Penzias P. Spatial Coverage and Temporal Trends of Land-based Atmospheric Mercury Measurements in the Northern and Southern Hemispheres. Mercury Fate and Transport in the Global Atmosphere: Emissions, Measurements, and Models. Springer Verlag, New York, 2009, pp. 223.

Ebinghaus R, Jennings SG, Kock HH, Derwent RG, Manning AJ, Spain TG. Decreasing trends in total gaseous mercury observations in baseline air at Mace Head, Ireland from 1996 to 2009. Atmos. Environ. 2011; 45: 3475-3480.

Eckley C, Gustin M, Marsik F, Miller M. Measurement of surface mercury fluxes at active industrial gold mines in Nevada (USA). Sci. Total Environ. 2011; 409: 514-522.

Eckley CS, Gustin M, Lin CJ, Li X, Miller MB. The influence of dynamic chamber design and operating parameters on calculated surface-to-air mercury fluxes. Atmos. Environ. 2010; 44: 194-203.

Edgerton ES, Hartsell BE, Jansen JJ. Mercury speciation in coal-fired power plant plumes observed at three surface sites in the southeastern US. Environ. Sci. Technol. 2006; 40: 4563-4570.

El-Feky AA, El-Azab W, Ebiad MA, Masod MB, Faramawy S. Monitoring of elemental mercury in ambient air around an Egyptian natural gas processing plant. J. Nat. Gas Sci. Eng. 2018; 54: 189-201.

Engle MA, Tate MT, Krabbenhoft DP, Schauer JJ, Kolker A, Shanley JB, Bothner MH. Comparison of atmospheric mercury speciation and deposition at nine sites across central and eastern North America. J. Geophys. Res. Atmos. 2010; 115.

Enrico M, Roux GL, Marusczak N, Heimbürger LE, Claustres A, Fu X, Sun R, Sonke JE. Atmospheric Mercury Transfer to Peat Bogs Dominated by Gaseous Elemental Mercury Dry Deposition. Environ. Sci. Technol. 2016; 50: 2405-2412.

Fain X, Obrist D, Hallar AG, McCubbin I, Rahn T. High levels of reactive gaseous mercury observed at a high elevation research laboratory in the Rocky Mountains. Atmos. Chem. Phys. 2009; 9: 8049-8060.

Faïn X, Obrist D, Pierce A, Barth C, Gustin MS, Boyle DP. Whole-watershed mercury balance at Sagehen Creek, Sierra Nevada, CA. Geochim. Cosmochim. Acta 2011; 75: 2379-2392.

Fang G-C, Kao C-L, Huang P-W, Chen H-M, Wu Y-L, Liang G-R. Particulates and particulates-bound mercury (Hg (p)) sizes (PM 18, PM 10, PM 2.5, PM 1, PM< 1) distributions study by using MOUDI sampler at a complex sampling site. Environ. Geochem. Health 2019: 1-11.

Fang G-C, Lo C-T, Liu C-K. Seasonal variations (autumn, winter, and spring) of atmospheric particulate and particulate-bound mercury Hg (p) at a suburban/coastal area. Environ. Forsensics 2010; 11: 300-308.

Fang G, Zhang L, Huang C. Measurements of size-fractionated concentration and bulk dry deposition of atmospheric particulate bound mercury. Atmos. Environ. 2012; 61: 371-377.

Fang GC, Lo CT, Cho MH, Zhuang YJ, Tsai KH, Huang CY, Xiao YF. Annual ambient atmospheric mercury speciation measurement from Longjing, a rural site in Taiwan. Environ. Geochem. Health 2017; 39: 901-911.

Fang GC, Tsai KH, Huang CY, Yang KPO, Xiao YF, Huang WC, Zhuang YJ. Seasonal variations of ambient air mercury species nearby an airport. Atmos. Res. 2018; 202: 96-104.

Feddersen D, Talbot R, Mao H, Sive B. Size distribution of particulate mercury in marine and coastal atmospheres. Atmos. Chem. Phys. 2012; 12: 10899-10909.

Feng XB, Sommar J, Gardfeldt K, Lindqvist O. Improved determination of gaseous divalent mercury in ambient air using KCl coated denuders. Fresenius J. Anal. Chem. 2000; 366: 423-428.

Fritsche J, Obrist D, Zeeman MJ, Conen F, Eugster W, Alewell C. Elemental mercury fluxes over a sub-alpine grassland determined with two micrometeorological methods. Atmos. Environ. 2008; 42: 2922-2933.

Fu X, Feng X, Shang L, Wang S, Zhang H. Two years of measurements of atmospheric total gaseous mercury (TGM) at a remote site in Mt. Changbai area, Northeastern China. Atmos. Chem. Phys. 2012a; 12: 4215-4226.

Fu X, Feng X, Sommar J, Wang S. A review of studies on atmospheric mercury in China. Sci. Total Environ. 2012b; 421: 73-81.

Fu X, Zhang H, Yu B, Wang X, Lin C, Feng X. Observations of atmospheric mercury in China: a critical review. Atmos. Chem. Phys. 2015; 15: 9455-9476.

Gencarelli CN, Bieser J, Carbone F, De Simone F, Hedgecock IM, Matthias V, Travnikov O, Yang X, Pirrone N. Sensitivity model study of regional mercury dispersion in the atmosphere. Atmos. Chem. Phys. 2017; 17: 627-643.

Gerson JR, Driscoll CT, Demers JD, Sauer AK, Blackwell BD, Montesdeoca MR, Shanley JB, Ross DS. Deposition of mercury in forests across a montane elevation gradient: Elevational and seasonal patterns in methylmercury inputs and production. J. Geophys. Res. Biogeosci. 2017; 122: 1922-1939.

Goodsite ME, Plane J, Skov H. A theoretical study of the oxidation of Hg0 to HgBr2 in the troposphere. Environ. Sci. Technol. 2004; 38: 1772-1776.

Gratz L, Ambrose J, Jaffe D, Shah V, Jaeglé L, Stutz J, Festa J, Spolaor M, Tsai C, Selin N, Song S, Zhou X, Weinheimer A, Knapp DJ, Montzka DD, Flocke F, Campos T, Apel EC, Hornbrook RS, Blake N, Hall S, Tyndall G, Reeves M, Stechman D, Stell M. Oxidation of mercury by bromine in the subtropical Pacific free troposphere. Geophys. Res. Lett. 2015a; 42: 10494–10502.

Gratz L, Jaffe D, Hee J. Causes of increasing ozone and decreasing carbon monoxide in springtime at the Mt. Bachelor Observatory from 2004 to 2013. Atmos. Environ. 2015b; 109: 323-330.

Gratz LE, Eckley CS, Schwantes SJ, Mattson E. Ambient Mercury Observations near a Coal-Fired Power Plant in a Western US Urban Area. Atmosphere 2019; 10: 176.

Gratz LE, Keeler GJ. Sources of mercury in precipitation to Underhill, VT. Atmos. Environ. 2011; 45: 5440-5449.

Gratz LE, Keeler GJ, Miller EK. Long-term relationships between mercury wet deposition and meteorology. Atmos. Environ. 2009; 43: 6218-6229.

Gratz LE, Keeler GJ, Morishita M, Barres JA, Dvonch JT. Assessing the emission sources of atmospheric mercury in wet deposition across Illinois. Sci. Total Environ. 2013; 448: 120-131.

Grigal D. Inputs and outputs of mercury from terrestrial watersheds: a review. Environ. Rev. 2002; 10: 1-39.

Guentzel J, Landing W, Gill G, Pollman C. Atmospheric deposition of mercury in Florida: the FAMS project (1992–1994). Mercury as a Global Pollutant. Springer, 1995, pp. 393-402.

Guentzel JL, Landing WM, Gill GA, Pollman CD. Processes influencing rainfall deposition of mercury in Florida. Environ. Sci. Technol. 2001; 35: 863-873.

Guo J, Kang S, Huang J, Zhang Q, Rupakheti M, Sun S, Tripathee L, Rupakheti D, Panday AK, Sillanpää M, Paudyal R. Characterizations of atmospheric particulate-bound mercury in the Kathmandu Valley of Nepal, South Asia. Sci. Total Environ. 2017; 579: 1240-1248.

Guo Y, Feng X, Li Z, He T, Yan H, Meng B, Zhang J, Qiu G. Distribution and wet deposition fluxes of total and methyl mercury in Wujiang River Basin, Guizhou, China. Atmos. Environ. 2008; 42: 7096-7103.

Gustin M, Dunham-Cheatham SM, Zhang L. Comparison of four methods for measurement of reactive, gaseous oxidized, and particulate bound mercury. Environ. Sci. Technol. 2019; *submitted*.

Gustin M, Weiss-Penzias PS, Peterson C. Investigating sources of gaseous oxidized mercury in dry deposition at three sites across Florida, USA. Atmos. Chem. Phys. 2012; 12: 9201-9219.

Gustin MS, Amos HM, Huang J, Miller MB, Heidecorn K. Measuring and modeling mercury in the atmosphere: a critical review. Atmos. Chem. Phys. 2015; 15: 5697-5713.

Gustin MS, Huang J, Miller MB, Peterson C, Jaffe DA, Ambrose J, Finley BD, Lyman SN, Call K, Talbot R, Feddersen D, Mao H, Lindberg S. Do we understand what the mercury speciation instruments are actually measuring? Results of RAMIX. Environ. Sci. Technol. 2013; 47: 7295-7306.

Gustin MS, Lindberg SE, Weisberg PJ. An update on the natural sources and sinks of atmospheric mercury. Appl. Geochem. 2008; 23: 482-493.

Gustin MS, Pierce AM, Huang J, Miller MB, Holmes H, Loria-Salazar SM. Evidence for different reactive Hg sources and chemical compounds at adjacent valley and high elevation locations. Environ. Sci. Technol. 2016; DOI: 10.1021/acs.est.6b03339.

Hall B. The gas phase oxidation of elemental mercury by ozone. Mercury as a Global Pollutant. Springer, 1995, pp. 301-315.

Hall B, Olson M, Rutter A, Frontiera R, Krabbenhoft D, Gross D, Yuen M, Rudolph T, Schauer J. Atmospheric mercury speciation in Yellowstone National Park. Sci. Total Environ. 2006; 367: 354-366.

Hall NL, Dvonch JT, Marsik FJ, Barres JA, Landis MS. An artificial turf-based surrogate surface collector for the direct measurement of atmospheric mercury dry deposition. Int. J. Environ. Res. Public Health 2017; 14.

Hammerschmidt CR, Fitzgerald WF. Methylmercury in freshwater fish linked to atmospheric mercury deposition. Environ. Sci. Technol. 2006; 40: 7764-7770.

Hammerschmidt CR, Lamborg CH, Fitzgerald WF. Aqueous phase methylation as a potential source of methylmercury in wet deposition. Atmos. Environ. 2007; 41: 1663-1668.

Han D, Zhang J, Hu Z, Ma Y, Duan Y, Han Y, Chen X, Zhou Y, Cheng J, Wang W. Particulate mercury in ambient air in Shanghai, China: Size-specific distribution, gas–particle partitioning, and association with carbonaceous composition. Environ. Pollut. 2018; 238: 543-553.

Hartmann DL, Klein Tank AMG, Rusticucci M, Alexander LV, Brönnimann S, Charabi YAR, Dentener FJ, Dlugokencky EJ, Easterling DR, Kaplan A, Soden BJ, Thorne PW, Wild M, Zhai P. Observations: Atmosphere and surface. Climate Change 2013 the Physical Science Basis: Working Group I Contribution to the Fifth Assessment Report of the Intergovernmental Panel on Climate Change. 9781107057999, 2013, pp. 159-254.

Hedgecock IM, Pirrone N, Sprovieri F, Pesenti E. Reactive gaseous mercury in the marine boundary layer: Modelling and experimental evidence of its formation in the Mediterranean region. Atmos. Environ. 2003; 37: 41-49.

Hennigan CJ, Bergin MH, Dibb JE, Weber RJ. Enhanced secondary organic aerosol formation due to water uptake by fine particles. Geophys. Res. Lett. 2008; 35.

Henny CJ, Hill EF, Hoffman DJ, Spalding MG, Grove RA. Nineteenth century mercury: hazard to wading birds and cormorants of the Carson River, Nevada. Ecotoxicology 2002; 11: 213-231.

Heyes A, Mason RP, Kim E-H, Sunderland E. Mercury methylation in estuaries: Insights from using measuring rates using stable mercury isotopes. Mar. Chem. 2006; 102: 134-147.

Hoglind H, Eriksson S, Gardfeldt K. Ship-based measurements of atmospheric mercury concentrations over the Baltic Sea. Atmosphere 2018; 9.

Holmes CD, Jacob DJ, Corbitt ES, Mao J, Yang X, Talbot R, Slemr F. Global atmospheric model for mercury including oxidation by bromine atoms. Atmos. Chem. Phys. 2010; 10: 12037-12057.

Holmes CD, Jacob DJ, Mason RP, Jaffe DA. Sources and deposition of reactive gaseous mercury in the marine atmosphere. Atmos. Environ. 2009; 43: 2278-2285.

Holmes CD, Krishnamurthy NP, Caffrey JM, Landing WM, Edgerton ES, Knapp KR, Nair US. Thunderstorms increase mercury wet deposition. Environ. Sci. Technol. 2016; 50: 9343-9350.

Horowitz HM, Jacob DJ, Zhang Y, Dibble TS, Slemr F, Amos HM, Schmidt JA, Corbitt ES, Marais EA, Sunderland EM. A new mechanism for atmospheric mercury redox chemistry: Implications for the global mercury budget. Atmos. Chem. Phys. 2017; 17: 6353-6371.

Houston MC. Role of mercury toxicity in hypertension, cardiovascular disease, and stroke. J. Clin. Hypertens. 2011; 13: 621-627.

Howard D, Edwards GC. Mercury fluxes over an Australian alpine grassland and observation of nocturnal atmospheric mercury depletion events. Atmos. Chem. Phys. 2018; 18: 129-142.

Howard D, Nelson PF, Edwards GC, Morrison AL, Fisher JA, Ward J, Harnwell J, Schoot Mvd, Atkinson B, Chambers SD. Atmospheric mercury in the Southern Hemisphere tropics: seasonal and diurnal variations and influence of inter-hemispheric transport. Atmos. Chem. Phys. 2017; 17: 11623-11636.

Hoyer M, Burke J, Keeler G. Atmospheric sources, transport and deposition of mercury in Michigan: two years of event precipitation. Water, Air, Soil Pollut. 1995; 80: 199-208.

Huang J, Gustin MS. Evidence for a free troposphere source of mercury in wet deposition in the Western United States. Environ. Sci. Technol. 2012; 46: 6621-6629.

Huang J, Gustin MS. Uncertainties of Gaseous Oxidized Mercury Measurements Using KCl-Coated Denuders, Cation-Exchange Membranes, and Nylon Membranes: Humidity Influences. Environ. Sci. Technol. 2015; 49: 6102-6108.

Huang J, Lyman SN, Hartman JS, Gustin MS. A review of passive sampling systems for ambient air mercury measurements. Environ. Sci. Proc. Imp. 2014; 16: 374-392.

Huang J, Miller MB, Edgerton E, Gustin MS. Use of criteria pollutants, active and passive mercury sampling, and receptor modeling to understand the chemical forms of gaseous oxidized mercury in Florida. Atmos. Chem. Phys. Discuss. 2015; 15: 12069-12105.

Huang J, Miller MB, Edgerton E, Sexauer Gustin M. Deciphering potential chemical compounds of gaseous oxidized mercury in Florida, USA. Atmos. Chem. Phys. 2017; 17: 1689-1698.

Huang J, Miller MB, Weiss-Penzias P, Gustin MS. Comparison of gaseous oxidized Hg measured by KCl-coated denuders, and nylon and cation exchange membranes. Environ. Sci. Technol. 2013; 47: 7307-7316.

Huber ML, Laesecke A, Friend DG. Correlation for the vapor pressure of mercury. Ind. Eng. Chem. Res. 2006; 45: 7351-7361.

Hynes AJ, Donohoue DL, Goodsite ME, Hedgecock IM. Our current understanding of major chemical and physical processes affecting mercury dynamics in the atmosphere and at the air-water/terrestrial interfaces. In: Mason R, Pirrone N, editors. Mercury Fate and Transport in the Global Atmosphere. Springer US, 2009, pp. 427-457; 457.

Hynes AJ, Everhart S, Bauer D, Remeika J, Tatum Ernest C. In situ and denuder-based measurements of elemental and reactive gaseous mercury with analysis by laser-induced fluorescence – results from the Reno Atmospheric Mercury Intercomparison Experiment. Atmos. Chem. Phys. 2017a; 17: 465-483.

Hynes AJ, Everhart S, Bauer D, Remeika J, Tatum Ernest C. In situ and denuder-based measurements of elemental and reactive gaseous mercury with analysis by laser-induced fluorescence – results from the Reno Atmospheric Mercury Intercomparison Experiment. Atmos. Chem. Phys. 2017b; 17: 465-483.

Jaffe DA, Lyman S, Amos HM, Gustin MS, Huang J, Selin NE, Levin L, Ter Schure A, Mason RP, Talbot R, Rutter A, Finley B, Jaeglé L, Shah V, McClure CD, Ambrose JL, Gratz L, Lindberg S, Weiss-Penzias P, Sheu GR, Feddersen D, Horvat M, Dastoor A, Hynes A, Mao H, Sonke JE, Slemr F, Fisher JA, Ebinghaus R, Zhang Y, Edwards G. Progress on understanding atmospheric mercury hampered by uncertain measurements. Environ. Sci. Technol. 2014; 48: 7204-7206.

Jiao Y, Dibble TS. First kinetic study of the atmospherically important reactions BrHg+ NO 2 and BrHg+ HOO. Phys. Chem. Chem. Phys. 2017a; 19: 1826-1838.

Jiao Y, Dibble TS. Structures, Vibrational Frequencies, and Bond Energies of the BrHgOX and BrHgXO Species Formed in Atmospheric Mercury Depletion Events. J. Phys. Chem. A 2017b; 121: 7976-7985.

Jiskra M, Sonke JE, Obrist D, Bieser J, Ebinghaus R, Myhre CL, Pfaffhuber KA, Wängberg I, Kyllönen K, Worthy D, Martin LG, Labuschagne C, Mkololo T, Ramonet M, Magand O, Dommergue A. A vegetation control on seasonal variations in global atmospheric mercury concentrations. Nature Geosci. 2018; 11: 244-250.

Jones CP, Lyman SN, Jaffe DA, Allen T, O'Neil TL. Detection and quantification of gas-phase oxidized mercury compounds by GC/MS. Atmos. Meas. Tech. 2016; 9: 2195-2205.

Kalinchuk V, Lopatnikov E, Astakhov A. Gradient measurements of gaseous elemental mercury (Hg0) in the marine boundary layer of the northwest Sea of Japan (East Sea). Environ. Pollut. 2018a; 237: 1124-1136.

Kalinchuk VV, Mishukov VF, Astakhov AS. Arctic source for elevated atmospheric mercury (Hg0) in the western Bering Sea in the summer of 2013. J. Environ. Sci. 2018b; 68: 114-121.

Kamp J, Skov H, Jensen B, Sørensen LL. Fluxes of gaseous elemental mercury (GEM) in the High Arctic during atmospheric mercury depletion events (AMDEs). Atmos. Chem. Phys. 2018; 18: 6923-6938.

Karthik R, Paneerselvam A, Ganguly D, Hariharan G, Srinivasalu S, Purvaja R, Ramesh R. Temporal variability of atmospheric Total Gaseous Mercury and its correlation with meteorological parameters at a high-altitude station of the South India. Atmos. Pollut. Res. 2017; 8: 164-173.

Kaulfus AS, Nair U, Holmes CD, Landing WM. Mercury wet scavenging and deposition differences by precipitation type. Environ. Sci. Technol. 2017; 51: 2628-2634.

Keeler G, Glinsorn G, Pirrone N. Particulate mercury in the atmosphere: its significance, transport, transformation and sources. Water, Air, Soil Pollut. 1995; 80: 159-168.

Keeler GJ, Gratz LE, Al-Wali K. Long-term atmospheric mercury wet deposition at Underhill, Vermont. Ecotoxicology 2005; 14: 71-83.

Kim KH, Brown RJC, Kwon E, Kim IS, Sohn JR. Atmospheric mercury at an urban station in Korea across three decades. Atmos. Environ. 2016; 131: 124-132.

Kim P-R, Han Y-J, Holsen TM, Yi S-M. Atmospheric particulate mercury: Concentrations and size distributions. Atmos. Environ. 2012; 61: 94-102.

Kos G, Ryzhkov A, Dastoor A, Narayan J, Steffen A, Ariya P, Zhang L. Evaluation of discrepancy between measured and modelled oxidized mercury species. Atmos. Chem. Phys. 2013; 13: 4839-4863.

Krabbenhoft DP, Sunderland EM. Global change and mercury. Science 2013; 341: 1457-1458.

Kumari A, Kumar B, Manzoor S, Kulshrestha U. Status of atmospheric mercury research in South Asia: A review. Aerosol Air Qual. Res. 2015; 15: 1092-1109.

Lam KT, Wilhelmsen CJ, Schwid AC, Jiao Y, Dibble TS. Computational Study on the Photolysis of BrHgONO and the Reactions of BrHgO• with CH4, C2H6, NO, and NO2: Implications for Formation of Hg (II) Compounds in the Atmosphere. J. Phys. Chem. A 2019.

Landing W, Caffrey J, Nolek S, Gosnell K, Parker W. Atmospheric wet deposition of mercury and other trace elements in Pensacola, Florida. Atmos. Chem. Phys. 2010; 10: 4867-4877.

Landis MS, Keeler GJ. Critical evaluation of a modified automatic wet-only precipitation collector for mercury and trace element determinations. Environ. Sci. Technol. 1997; 31: 2610-2615.

Landis MS, Ryan JV, ter Schure AF, Laudal D. Behavior of mercury emissions from a commercial coal-fired power plant: The relationship between stack speciation and near-field plume measurements. Environ. Sci. Technol. 2014; 48: 13540-13548.

Landis MS, Vette AF, Keeler GJ. Atmospheric mercury in the Lake Michigan basin: influence of the Chicago/Gary urban area. Environ. Sci. Technol. 2002; 36: 4508-4517.

Lee GS, Kim PR, Han YJ, Holsen TM, Seo YS, Yi SM. Atmospheric speciated mercury concentrations on an island between China and Korea: Sources and transport pathways. Atmos. Chem. Phys. 2016; 16: 4119-4133.

Lei H, Liang XZ, Wuebbles DJ, Tao Z. Model analyses of atmospheric mercury: Present air quality and effects of transpacific transport on the United States. Atmos. Chem. Phys. 2013; 13: 10807-10825.

Li P, Feng X, Qiu G. Methylmercury exposure and health effects from rice and fish consumption: a review. Int. J. Environ. Res. Public Health 2010; 7: 2666-2691.

Li P, Feng X, Yuan X, Chan HM, Qiu G, Sun G-X, Zhu Y-G. Rice consumption contributes to low level methylmercury exposure in southern China. Environ. Int. 2012; 49: 18-23.

Li T, Wang Y, Mao H, Wang S, Talbot RW, Zhou Y, Wang Z, Nie X, Qie G. Insights on Chemistry of Mercury Species in Clouds over Northern China: Complexation and Adsorption. Environ. Sci. Technol. 2018; 52: 5125-5134.

Li Y, Wang Y, Li Y, Li T, Mao H, Talbot R, Nie X, Wu C, Zhao Y, Hou C, Wang G, Zhou J, Qie G. Characteristics and potential sources of atmospheric particulate mercury in Jinan, China. Sci. Total Environ. 2017; 574: 1424-1431.

Lian M, Shang L, Duan Z, Li Y, Zhao G, Zhu S, Qiu G, Meng B, Sommar J, Feng X, Svanberg S. Lidar mapping of atmospheric atomic mercury in the Wanshan area, China. Environ. Pollut. 2018; 240: 353-358.

Lin C-J, Pehkonen SO. The chemistry of atmospheric mercury: a review. Atmos. Environ. 1999; 33: 2067-2079.

Lin CJ, Pehkonen SO. Oxidation of elemental mercury by aqueous chlorine (HOCl/OCl−): Implications for tropospheric mercury chemistry. J. Geophys. Res. Atmos. 1998; 103: 28093-28102.

Lin CJ, Pongprueksa P, Lindberg SE, Pehkonen SO, Byun D, Jang C. Scientific uncertainties in atmospheric mercury models I: Model science evaluation. Atmos. Environ. 2006; 40: 2911-2928.

Lin H, Tong Y, Yin X, Zhang Q, Zhang H, Zhang H, Chen L, Kang S, Zhang W, Schauer J, De Foy B, Bu X, Wang X. First measurement of atmospheric mercury species in Qomolangma Natural Nature Preserve, Tibetan Plateau, and evidence of transboundary pollutant invasion. Atmos. Chem. Phys. 2019; 19: 1373-1391.

Lin H, Zhang W, Deng C, Tong Y, Zhang Q, Wang X. Evaluation of passive sampling of gaseous mercury using different sorbing materials. Environ. Sci. Pollut. Res. 2017; 24: 14190-14197.

Liu C, Fu X, Zhang H, Ming L, Xu H, Zhang L, Feng X. Sources and outflows of atmospheric mercury at Mt. Changbai, northeastern China. Sci. Total Environ. 2019; 663: 275-284.

Liu Y, Wu B, Hao Y, Zhu W, Li Z, Chai X. Site-specific diel mercury emission fluxes in landfill: combined effects of vegetation and meteorological factors. Waste Manage. 2017; 59: 247-254.

Lohman K, Seigneur C, Edgerton E, Jansen J. Modeling mercury in power plant plumes. Environ. Sci. Technol. 2006; 40: 3848-3854.

Lombard M, Bryce J, Mao H, Talbot R. Mercury deposition in southern New Hampshire, 2006–2009. Atmos. Chem. Phys. 2011; 11: 7657-7668.

Lyman S, Jones C, O'Neil T, Allen T, Miller M, Gustin MS, Pierce AM, Luke W, Ren X, Kelley P. Automated Calibration of Atmospheric Oxidized Mercury Measurements. Environ. Sci. Technol. 2016; 50: 12921-12927.

Lyman SN, Gustin MS, Prestbo EM, Marsik FJ. Estimation of Dry Deposition of Atmospheric Mercury in Nevada by Direct and Indirect Methods. Environ. Sci. Technol. 2007; 41: 1970-1976.

Lyman SN, Jaffe DA. Elemental and oxidized mercury in the upper troposphere and lower stratosphere. Nature Geosci. 2012; 5: 114-117.

Lyman SN, Jaffe DA, Gustin MS. Release of mercury halides from KCl denuders in the presence of ozone. Atmos. Chem. Phys. 2010; 10: 8197-8204.

Lynam M, Keeler G. Comparison of methods for particulate phase mercury analysis: sampling and analysis. Anal. Bioanal. Chem. 2002; 374: 1009-1014.

Lynam MM, Dvonch JT, Barres JA, Landis MS, Kamal AS. Investigating the impact of local urban sources on total atmospheric mercury wet deposition in Cleveland, Ohio, USA. Atmos. Environ. 2016; 127: 262-271.

Lynam MM, Keeler GJ. Artifacts associated with the measurement of particulate mercury in an urban environment: The influence of elevated ozone concentrations. Atmos. Environ. 2005; 39: 3081-3088.

Ma M, Wang D, Du H, Sun T, Zhao Z, Wei S. Atmospheric mercury deposition and its contribution of the regional atmospheric transport to mercury pollution at a national forest nature reserve, southwest China. Environ. Sci. Pollut. Res. 2015; 22: 20007-20018.

Macagnano A, Papa P, Avossa J, Perri V, Marelli M, Sprovieri F, Zampetti E, De Cesare F, Bearzotti A, Pirrone N. Passive sampling of gaseous elemental mercury based on a composite tio2np/aunp layer. Nanomaterials 2018; 8.

Macagnano A, Perri V, Zampetti E, Bearzotti A, De Cesare F, Sprovieri F, Pirrone N. A smart nanofibrous material for adsorbing and detecting elemental mercury in air. Atmos. Chem. Phys. 2017a; 17: 6883-6893.

Macagnano A, Perri V, Zampetti E, Ferretti AM, Sprovieri F, Pirrone N, Bearzotti A, Esposito G, De Cesare F. Elemental mercury vapor chemoresistors employing TIO2 nanofibers photocatalytically decorated with Au-nanoparticles. Sens. Actuators B Chem. 2017b; 247: 957-967.

Malcolm EG, Ford AC, Redding TA, Richardson MC, Strain BM, Tetzner SW. Experimental investigation of the scavenging of gaseous mercury by sea salt aerosol. J. Atmos. Chem. 2009; 63: 221-234.

Malcolm EG, Keeler GJ. Evidence for a sampling artifact for particulate-phase mercury in the marine atmosphere. Atmos. Environ. 2007; 41: 3352-3359.

Malcolm EG, Keeler GJ, Lawson ST, Sherbatskoy TD. Mercury and trace elements in cloud water and precipitation collected on Mt. Mansfield, Vermont. J. Environ. Monit. 2003; 5: 584-590.

Mamane Y, Perrino C, Yossef O, Catrambone M. Source characterization of fine and coarse particles at the East Mediterranean coast. Atmos. Environ. 2008; 42: 6114-6130.

Mao H, Cheng I, Zhang L. Current understanding of the driving mechanisms for spatiotemporal variations of atmospheric speciated mercury: A review. Atmos. Chem. Phys. 2016; 16: 12897-12924.

Mao H, Hall D, Ye Z, Zhou Y, Felton D, Zhang L. Impacts of large-scale circulation on urban ambient concentrations of gaseous elemental mercury in New York, USA. Atmos. Chem. Phys. 2017a; 17: 11655-11671.

Mao H, Talbot R, Hegarty J, Koermer J. Speciated mercury at marine, coastal, and inland sites in New England–Part 2: Relationships with atmospheric physical parameters. Atmos. Chem. Phys. 2012; 12: 4181-4206.

Mao H, Talbot RW, Sive BC, Youn Kim S, Blake DR, Weinheimer AJ. Arctic mercury depletion and its quantitative link with halogens. J. Atmos. Chem. 2010; 65: 1-26.

Mao H, Ye Z, Driscoll C. Meteorological effects on Hg wet deposition in a forested site in the Adirondack region of New York during 2000–2015. Atmos. Environ. 2017b; 168: 90-100.

Marsik FJ, Keeler GJ, Landis MS. The dry-deposition of speciated mercury to the Florida Everglades: Measurements and modeling. Atmos. Environ. 2007; 41: 136-149.

Martin LG, Labuschagne C, Brunke EG, Weigelt A, Ebinghaus R, Slemr F. Trend of atmospheric mercury concentrations at Cape Point for 1995-2004 and since 2007. Atmos. Chem. Phys. 2017; 17: 2393-2399.

Marumoto K, Matsuyama A. Mercury speciation in wet deposition samples collected from a coastal area of Minamata Bay. Atmos. Environ. 2014; 86: 220-227.

Marumoto K, Suzuki N, Shibata Y, Takeuchi A, Takami A, Fukuzaki N, Kawamoto K, Mizohata A, Kato S, Yamamoto T. Long-Term Observation of Atmospheric Speciated Mercury during 2007–2018 at Cape Hedo, Okinawa, Japan. Atmosphere 2019; 10: 362.

Marusczak N, Sonke JE, Fu X, Jiskra M. Tropospheric GOM at the Pic du Midi Observatory–correcting bias in denuder based observations. Environ. Sci. Technol. 2016; 51: 863-869.

Mason RP, Hammerschmidt CR, Lamborg CH, Bowman KL, Swarr GJ, Shelley RU. The air-sea exchange of mercury in the low latitude Pacific and Atlantic Oceans. Deep Sea Res. (I Oceanogr. Res. Pap.) 2017; 122: 17-28.

McClure CD, Jaffe DA, Edgerton ES. Evaluation of the KCl denuder method for gaseous oxidized mercury using HgBr2 at an in-service AMNet site. Environ. Sci. Technol. 2014; 48: 11437-11444.

McLagan DS, Mazur ME, Mitchell CP, Wania F. Passive air sampling of gaseous elemental mercury: a critical review. Atmos. Chem. Phys. 2016; 16: 3061-3076.

McLagan DS, Mitchell CPJ, Steffen A, Hung H, Shin C, Stupple GW, Olson ML, Luke WT, Kelley P, Howard D, Edwards GC, Nelson PF, Xiao H, Sheu GR, Dreyer A, Huang H, Abdul Hussain B, Lei YD, Tavshunsky I, Wania F. Global evaluation and calibration of a passive air sampler for gaseous mercury. Atmos. Chem. Phys. 2018; 18: 5905-5919.

Mergler D, Anderson HA, Chan LHM, Mahaffey KR, Murray M, Sakamoto M, Stern AH. Ambio 2007; 36: 3.

Michael R, Stuart AL, Trotz MA, Akiwumi F. Source apportionment of wet-deposited atmospheric mercury in Tampa, Florida. Atmos. Res. 2016; 170: 168-175.

Miller G, Quashnick J, Hebert V. Reaction rate of metallic mercury with hydroxyl radical in the gas phase. Abstracts of Papers of the American Chemical Society. 221. American Chemical Society, 2001, pp. U47-U47.

Miller MB, Dunham-Cheatham SM, Gustin MS, Edwards GC. Evaluation of cation exchange membrane performance under exposure to high Hg0 and HgBr2 concentrations. Atmos. Meas. Tech. 2019; 12: 1207-1217.

Monperrus M, Tessier E, Amouroux D, Leynaert A, Huonnic P, Donard O. Mercury methylation, demethylation and reduction rates in coastal and marine surface waters of the Mediterranean Sea. Mar. Chem. 2007; 107: 49-63.

Morrison KA, Kuhn ES, Watras CJ. Comparison of three methods of estimating atmospheric mercury deposition. Environ. Sci. Technol. 1995; 29: 571-576.

Morton-Bermea O, Garza-Galindo R, Hernández-Álvarez E, Ordoñez-Godínez SL, Amador-Muñoz O, Beramendi-Orosco L, Miranda J, Rosas-Pérez I. Atmospheric PM2.5 Mercury in the Metropolitan Area of Mexico City. Bull. Environ. Contam. Toxicol. 2018; 100: 588-592.

Muntean M, Janssens-Maenhout G, Song S, Selin NE, Olivier JG, Guizzardi D, Maas R, Dentener F. Trend analysis from 1970 to 2008 and model evaluation of EDGARv4 global gridded anthropogenic mercury emissions. Sci. Total Environ. 2014; 494: 337-350.

Murray LT, Mickley LJ, Kaplan JO, Sofen ED, Pfeiffer M, Alexander B. Factors controlling variability in the oxidative capacity of the troposphere since the Last Glacial Maximum. Atmos. Chem. Phys. 2014; 14: 3589-3622.

Navrátil T, Nováková T, Shanley JB, Rohovec J, Matoušková Š, Vaňková M, Norton SA. Larch Tree Rings as a Tool for Reconstructing 20th Century Central European Atmospheric Mercury Trends. Environ. Sci. Technol. 2018; 52: 11060-11068.

Nerentorp Mastromonaco MG, Gårdfeldt K, Langer S. Mercury flux over West Antarctic Seas during winter, spring and summer. Mar. Chem. 2017; 193: 44-54.

Nic M, Hovorka L, Jirat J, Kosata B, Znamenacek J. IUPAC compendium of chemical terminology-the gold book: International Union of Pure and Applied Chemistry, 2005.

Obrist D, Agnan Y, Jiskra M, Olson CL, Colegrove DP, Hueber J, Moore CW, Sonke JE, Helmig D. Tundra uptake of atmospheric elemental mercury drives Arctic mercury pollution. Nature 2017; 547: 201-204.

Obrist D, Kirk JL, Zhang L, Sunderland EM, Jiskra M, Selin NE. A review of global environmental mercury processes in response to human and natural perturbations: Changes of emissions, climate, and land use. Ambio 2018; 47: 116-140.

Obrist D, Tas E, Peleg M, Matveev V, Faïn X, Asaf D, Luria M. Bromine-induced oxidation of mercury in the mid-latitude atmosphere. Nature Geosci. 2011; 4: 22-26.

Oken E, Wright RO, Kleinman KP, Bellinger D, Amarasiriwardena CJ, Hu H, Rich-Edwards JW, Gillman MW. Maternal fish consumption, hair mercury, and infant cognition in a US cohort. Environ. Health Perspect. 2005; 113: 1376-1380.

Osterwalder S, Sommar J, Åkerblom S, Jocher G, Fritsche J, Nilsson MB, Bishop K, Alewell C. Comparative study of elemental mercury flux measurement techniques over a Fennoscandian boreal peatland. Atmos. Environ. 2018; 172: 16-25.

Pacyna JM, Travnikov O, Simone FD, Hedgecock IM, Sundseth K, Pacyna EG, Steenhuisen F, Pirrone N, Munthe J, Kindbom K. Current and future levels of mercury atmospheric pollution on a global scale. Atmos. Chem. Phys. 2016; 16: 12495-12511.

Pal B, Ariya PA. Gas-Phase HO-Initiated Reactions of Elemental Mercury: Kinetics, Product Studies, and Atmospheric Implications. Environ. Sci. Technol. 2004a; 38: 5555-5566.

Pal B, Ariya PA. Studies of ozone initiated reactions of gaseous mercury: kinetics, product studies, and atmospheric implications. Phys. Chem. Chem. Phys. 2004b; 6: 572-579.

Pandey SK, Kim K-H, Brown RJ. Measurement techniques for mercury species in ambient air. Trends Analyt. Chem. 2011; 30: 899-917.

Pankow JF. Common y-intercept and single compound regressions of gas-particle partitioning data vs 1/T. Atmos. Environ. 1991; 25: 2229-2239.

Pankow JF. Application of common y-intercept regression parameters for log Kp vs 1/T for predicting gas-particle partitioning in the urban environment. Atmos. Environ. 1992; 26: 2489-2497.

Papa P, Fratoddi I, Venditti I, Vichi F, Macagnano A, Zampetti E, Bearzotti A. Use of gold nanoparticles as substrate for diffusive monitoring of gaseous mercury. Materials 2018; 11.

Peleg M, Tas E, Matveev V, Obrist D, Moore CW, Gabay M, Luria M. Observational evidence for involvement of nitrate radicals in nighttime oxidation of mercury. Environ. Sci. Technol. 2015.

Peterson C, Alishahi M, Gustin MS. Testing the use of passive sampling systems for understanding air mercury concentrations and dry deposition across Florida, USA. Sci. Total Environ. 2012; 424: 297-307.

Pleuel K, Munthe J. Modelling the atmospheric mercury cycle-chemistry in fog droplets. Atmos. Environ. 1995; 29: 1441-1457.

Pongprueksa P, Lin C-J, Lindberg SE, Jang C, Braverman T, Bullock Jr OR, Ho TC, Chu H-W. Scientific uncertainties in atmospheric mercury models III: Boundary and initial conditions, model grid resolution, and Hg (II) reduction mechanism. Atmos. Environ. 2008; 42: 1828-1845.

Prestbo EM, Gay DA. Wet deposition of mercury in the US and Canada, 1996-2005: Results and analysis of the NADP mercury deposition network (MDN). Atmos. Environ. 2009; 43: 4223-4233.

Prete D, Davis M, Lu J. Factors affecting the concentration and distribution of gaseous elemental mercury in the urban atmosphere of downtown Toronto. Atmos. Environ. 2018; 192: 24-34.

Qie G, Wang Y, Wu C, Mao H, Zhang P, Li T, Li Y, Talbot R, Hou C, Yue T. Distribution and sources of particulate mercury and other trace elements in PM 2.5 and PM 10 atop Mount Tai, China. J. Environ. Manage. 2018; 215: 195-205.

Qin C, Wang Y, Peng Y, Wang D. Four-year record of mercury wet deposition in one typical industrial city in southwest China. Atmos. Environ. 2016; 142: 442-451.

Quétel CR, Zampella M, Brown RJC. Temperature dependence of Hg vapour mass concentration at saturation in air: New SI traceable results between 15 and 30°C. Trends Analyt. Chem. 2016; 85: 81-88.

Read KA, Neves LM, Carpenter LJ, Lewis AC, Fleming ZF, Kentisbeer J. Four years (2011-2015) of total gaseous mercury measurements from the Cape Verde Atmospheric Observatory. Atmos. Chem. Phys. 2017; 17: 5393-5406.

Risch MR, Kenski DM. Spatial patterns and temporal changes in atmospheric-mercury deposition for the Midwestern USA, 2001-2016. Atmosphere 2018; 9: 29.

Ritchie CD, Richards W, Arp PA. Mercury in fog on the Bay of Fundy (Canada). Atmos. Environ. 2006; 40: 6321-6328.

Roman P, Polkowska Ż, Namieśnik J. Sampling procedures in studies of cloud water composition: A review. Crit. Rev. Environ. Sci. Technol. 2013; 43: 1517-1555.

Rutter A, Shakya K, Lehr R, Schauer J, Griffin R. Oxidation of gaseous elemental mercury in the presence of secondary organic aerosols. Atmos. Environ. 2012; 59: 86-92.

Rutter AP, Hanford KL, Zwers JT, Perillo-Nicholas AL, Schauer JJ, Olson ML. Evaluation of an offline method for the analysis of atmospheric reactive gaseous mercury and particulate mercury. J. Air Waste Manage. Assoc. 2008; 58: 377-383.

Rutter AP, Schauer JJ. The effect of temperature on the gas-particle partitioning of reactive mercury in atmospheric aerosols. Atmos. Environ. 2007a; 41: 8647-8657.

Rutter AP, Schauer JJ. The impact of aerosol composition on the particle to gas partitioning of reactive mercury. Environ. Sci. Technol. 2007b; 41: 3934-3939.

Saiz-Lopez A, Acuña AU, Trabelsi T, Carmona-García J, Dávalos JZ, Rivero D, Cuevas CA, Kinnison DE, Sitkiewicz SP, Roca-Sanjuán D. Gas-Phase Photolysis of Hg (I) Radical Species: A New Atmospheric Mercury Reduction Process. J. Am. Chem. Soc. 2019.

Saiz-Lopez A, Sitkiewicz SP, Roca-Sanjuán D, Oliva-Enrich JM, Dávalos JZ, Notario R, Jiskra M, Xu Y, Wang F, Thackray CP, Sunderland EM, Jacob DJ, Travnikov O, Cuevas CA, Acuña AU, Rivero D, Plane JMC, Kinnison DE, Sonke JE. Photoreduction of gaseous oxidized mercury changes global atmospheric mercury speciation, transport and deposition. Nat. Commun. 2018; 9: 4796.

Sakata M, Asakura K. Estimating contribution of precipitation scavenging of atmospheric particulate mercury to mercury wet deposition in Japan. Atmos. Environ. 2007; 41: 1669-1680.

Sakata M, Marumoto K. Wet and dry deposition fluxes of mercury in Japan. Atmos. Environ. 2005; 39: 3139-3146.

Sanei H, Outridge P, Goodarzi F, Wang F, Armstrong D, Warren K, Fishback L. Wet deposition mercury fluxes in the Canadian sub-Arctic and southern Alberta, measured using an automated precipitation collector adapted to cold regions. Atmos. Environ. 2010; 44: 1672-1681.

Santos EB, Ferlin S, Fostier AH, Mazali IO. Using gold nanoparticles as passive sampler for indoor monitoring of gaseous elemental mercury. J. Braz. Chem. Soc. 2017; 28: 1274-1280.

Sather ME, Mukerjee S, Smith L, Mathew J, Jackson C, Callison R, Scrapper L, Hathcoat A, Adam J, Keese D, Ketcher P, Brunette R, Karlstrom J, Ven der Jagt G. Gaseous oxidized mercury dry deposition

measurements in the Four Corners area and Eastern Oklahoma, USA. Atmos. Pollut. Res. 2013; 4: 168-180.

Schwindt AR, Fournie JW, Landers DH, Schreck CB, Kent ML. Mercury concentrations in salmouids from western US National Parks and relationships with age and macrophage aggregates. Environ. Sci. Technol. 2008; 42: 1365-1370.

Seigneur C, Abeck H, Chia G, Reinhard M, Bloom NS, Prestbo E, Saxena P. Mercury adsorption to elemental carbon (soot) particles and atmospheric particulate matter. Atmos. Environ. 1998; 32: 2649-2657.

Seigneur C, Vijayaraghavan K, Lohman K. Atmospheric mercury chemistry: Sensitivity of global model simulations to chemical reactions. J. Geophys. Res. Atmos. 2006; 111.

Selin NE. Global change and mercury cycling: Challenges for implementing a global mercury treaty. Environ. Toxicol. Chem. 2014; 33: 1202-1210.

Selin NE, Jacob DJ. Seasonal and spatial patterns of mercury wet deposition in the United States: Constraints on the contribution from North American anthropogenic sources. Atmos. Environ. 2008; 42: 5193-5204.

Selin NE, Javob DJ, Park RJ, Yantosca RM, Strode S, Jaeglé L, Jaffe D. Chemical cycling and deposition of atmospheric mercury: Global constraints from observations. J. Geophys. Res. Atmos. 2007; 112: D02308.

Seo Y-S, Han Y-J, Choi H-D, Holsen TM, Yi S-M. Characteristics of total mercury (TM) wet deposition: scavenging of atmospheric mercury species. Atmos. Environ. 2012; 49: 69-76.

Shah V, Jaeglé L. Subtropical subsidence and surface deposition of oxidized mercury produced in the free troposphere. Atmos. Chem. Phys. 2017; 17: 8999-9017.

Shah V, Jaeglé L, Gratz L, Ambrose J, Jaffe D, Selin N, Song S, Campos T, Flocke F, Reeves M, Stechman D, Stell M, Festa J, Stutz J, Weinheimer A, Knapp DJ, Montzka DD, Tyndall G, Apel EC, Hornbrook RS, Hills AJ, Riemer DD, Blake N, Cantrell CA, Mauldin RL. Origin of oxidized mercury in the summertime free troposphere over the southeastern US. Atmos. Chem. Phys. 2016; 16: 1511-1530.

Shanley JB, Engle MA, Scholl M, Krabbenhoft DP, Brunette R, Olson ML, Conroy ME. High mercury wet deposition at a “clean air” site in Puerto Rico. Environ. Sci. Technol. 2015; 49: 12474-12482.

Shen H, Tsai CM, Yuan CS, Jen YH, Ie IR. How incense and joss paper burning during the worship activities influences ambient mercury concentrations in indoor and outdoor environments of an Asian temple? Chemosphere 2017; 167: 530-540.

Sheu G-R, Lin N-H. Mercury in cloud water collected on Mt. Bamboo in northern Taiwan during the northeast monsoon season. Atmos. Environ. 2011; 45: 4454-4462.

Si L, Ariya PA. Recent advances in atmospheric chemistry of mercury. Atmosphere 2018; 9.

Simon H, Reff A, Wells B, Xing J, Frank N. Ozone trends across the United States over a period of decreasing NOx and VOC emissions. Environ. Sci. Technol. 2014; 49: 186-195.

Sitkiewicz SP, Oliva JM, Dávalos JZ, Notario R, Saiz–Lopez A, Alcoba DR, Oña OB, Roca-Sanjuán D. Ab initio quantum–chemical computations of the electronic states in HgBr2 and IBr: Molecules of interest on the Earth’s atmosphere. The Journal of chemical physics 2016; 145: 244304.

Sitkiewicz SP, Rivero D, Oliva-Enrich JM, Saiz-Lopez A, Roca-Sanjuán D. Ab initio quantum-chemical computations of the absorption cross sections of HgX 2 and HgXY (X, Y= Cl, Br, and I): molecules of interest in the Earth's atmosphere. Phys. Chem. Chem. Phys. 2019; 21: 455-467.

Siudek P, Kurzyca I, Siepak J. Atmospheric deposition of mercury in central Poland: sources and seasonal trends. Atmos. Res. 2016; 170: 14-22.

Sizmur T, McArthur G, Risk D, Tordon R, O'Driscoll NJ. Gaseous mercury flux from salt marshes is mediated by solar radiation and temperature. Atmos. Environ. 2017; 153: 117-125.

Slemr F, Brunke E-G, Ebinghaus R, Kuss J. Worldwide trend of atmospheric mercury since 1995. Atmos. Chem. Phys. 2011; 11: 4779-4787.

Slemr F, Ebinghaus R, Brenninkmeijer CAM, Hermann M, Kock HH, Martinsson BG, Schuck T, Sprung D, van Velthoven P, Zahn A, Ziereis H. Gaseous mercury distribution in the upper troposphere and lower stratosphere observed onboard the CARIBIC passenger aircraft. Atmos. Chem. Phys. 2009; 9: 1957-1969.

Slemr F, Weigelt A, Ebinghaus R, Bieser J, Brenninkmeijer CAM, Rauthe-Schöch A, Hermann M, Martinsson BG, Van Velthoven P, Bönisch H, Neumaier M, Zahn A, Ziereis H. Mercury distribution in the upper troposphere and lowermost stratosphere according to measurements by the IAGOS-CARIBIC observatory: 2014-2016. Atmos. Chem. Phys. 2018; 18: 12329-12343.

Snider G, Raofie F, Ariya PA. Effects of relative humidity and CO (g) on the O 3-initiated oxidation reaction of Hg 0 (g): kinetic & product studies. Phys. Chem. Chem. Phys. 2008; 10: 5616-5623.

Soerensen AL, Jacob DJ, Streets DG, Witt MLI, Ebinghaus R, Mason RP, Andersson M, Sunderland EM. Multi-decadal decline of mercury in the North Atlantic atmosphere explained by changing subsurface seawater concentrations. Geophys. Res. Lett. 2012; 39: L21810.

Sommar J, Gårdfeldt K, Strömberg D, Feng X. A kinetic study of the gas-phase reaction between the hydroxyl radical and atomic mercury. Atmos. Environ. 2001; 35: 3049-3054.

Spolaor A, Angot H, Roman M, Dommergue A, Scarchilli C, Vardè M, Del Guasta M, Pedeli X, Varin C, Sprovieri F. Feedback mechanisms between snow and atmospheric mercury: Results and observations from field campaigns on the Antarctic plateau. Chemosphere 2018; 197: 306-317.

Sprovieri F, Pirrone N, Bencardino M, D'Amore F, Angot H, Barbante C, Brunke E-G, Arcega-Cabrera F, Cairns W, Comero S. Five-year records of mercury wet deposition flux at GMOS sites in the Northern and Southern hemispheres. Atmos. Chem. Phys. 2017; 17: 2689-2708.

Sprovieri F, Pirrone N, Bencardino M, D'Amore F, Carbone F, Cinnirella S, Mannarino V, Landis M, Ebinghaus R, Weigelt A, Brunke EG, Labuschagne C, Martin L, Munthe J, Wangberg I, Artaxo P, Morais F, Barbosa HM, Brito J, Cairns W, Barbante C, Dieguez MC, Garcia PE, Dommergue A, Angot H, Magand O, Skov H, Horvat M, Kotnik J, Read KA, Neves LM, Gawlik BM, Sena F, Mashyanov N, Obolkin V, Wip D, Feng XB, Zhang H, X. F, Ramachandran R, Cossa D, Knoery J, Marusczak N, Nerentorp M, Norstrom C. Atmospheric Mercury Concentrations observed at ground-based monitoring sites globally distributed in the framework of the GMOS network. Atmos. Chem. Phys. 2016; 16: 11915-11935.

Sprovieri F, Pirrone N, Ebinghaus R, Kock H, Dommergue A. A review of worldwide atmospheric mercury measurements. Atmos. Chem. Phys. 2010; 10: 8245-8265.

Spry DJ, Wiener JG. Metal bioavailability and toxicity to fish in low-alkalinity lakes: a critical review. Environ. Pollut. 1991; 71: 243-304.

Srivastava A, Hodges JT. Development of a High-Resolution Laser Absorption Spectroscopy Method with Application to the Determination of Absolute Concentration of Gaseous Elemental Mercury in Air. Anal. Chem. 2018; 90: 6781-6788.

Stamenkovic J, Gustin MS. Nonstomatal versus stomatal uptake of atmospheric mercury. Environ. Sci. Technol. 2009; 43: 1367-1372.

Steffen A, Bottenheim J, Cole A, Douglas TA, Ebinghaus R, Friess U, Netcheva S, Nghiem S, Sihler H, Staebler R. Atmospheric mercury over sea ice during the OASIS-2009 campaign. Atmos. Chem. Phys. 2013; 13: 7007-7021.

Steffen A, Douglas T, Amyot M, Ariya P, Aspmo K, Berg T, Bottenheim J, Brooks S, Cobbett F, Dastoor A. A synthesis of atmospheric mercury depletion event chemistry in the atmosphere and snow. Atmos. Chem. Phys. 2008; 8: 1445-1482.

Steffen A, Lehnherr I, Cole A, Ariya P, Dastoor A, Durnford D, Kirk J, Pilote M. Atmospheric mercury in the Canadian Arctic. Part I: A review of recent field measurements. Sci. Total Environ. 2015; 509: 3-15.

Stern GA, Macdonald RW, Outridge PM, Wilson S, Chetelat J, Cole A, Hintelmann H, Loseto LL, Steffen A, Wang F. How does climate change influence arctic mercury? Sci. Total Environ. 2012; 414: 22-42.

Streets DG, Horowitz HM, Jacob DJ, Lu Z, Levin L, Ter Schure AFH, Sunderland EM. Total Mercury Released to the Environment by Human Activities. Environ. Sci. Technol. 2017; 51: 5969-5977.

Streets DG, Horowitz HM, Lu Z, Levin L, Thackray CP, Sunderland EM. Global and regional trends in mercury emissions and concentrations, 2010–2015. Atmos. Environ. 2019: 417-427.

Stylo M, Alvarez J, Dittkrist J, Jiao H. Global review of Mercury Monitoring Networks. United Nations Environmental Program, Geneva, Switzerland, 2016.

Subir M, Ariya PA, Dastoor AP. A review of uncertainties in atmospheric modeling of mercury chemistry I. Uncertainties in existing kinetic parameters–Fundamental limitations and the importance of heterogeneous chemistry. Atmos. Environ. 2011; 45: 5664-5676.

Subir M, Ariya PA, Dastoor AP. A review of the sources of uncertainties in atmospheric mercury modeling II. Mercury surface and heterogeneous chemistry–A missing link. Atmos. Environ. 2012; 46: 1-10.

Sun G, Sommar J, Feng X, Lin C-J, Ge M, Wang W, Yin R, Fu X, Shang L. Mass-dependent and-independent fractionation of mercury isotope during gas-phase oxidation of elemental mercury vapor by atomic Cl and Br. Environ. Sci. Technol. 2016; 50: 9232-9241.

Swartzendruber PC, Jaffe DA, Prestbo EM, Weiss-Penzias P, Selin NE, Park R, Jacob DJ, Strode S, Jaeglé L. Observations of reactive gaseous mercury in the free troposphere at the Mt. Bachelor Observatory. J. Geophys. Res. Atmos. 2006; 111: D24301.

Tacey SA, Xu L, Mavrikakis M, Schauer JJ. Heterogeneous Reduction Pathways for Hg (II) Species on Dry Aerosols: A First-Principles Computational Study. J. Phys. Chem. A 2016; 120: 2106-2113.

Talbot R, Mao H, Feddersen D, Smith M, Kim SY, Sive B, Haase K, Ambrose J, Zhou Y, Russo R. Comparison of Particulate Mercury Measured with Manual and Automated Methods. Atmosphere 2011; 2: 1-20.

Tang Y, Wang S, Wu Q, Liu K, Li Z, Zou J, Hou D, Wu Y, Duan L. Measurement of size-fractionated particulate-bound mercury in Beijing and implications on sources and dry deposition of mercury. Sci. Total Environ. 2019; 675: 176-183.

Tang Y, Wang S, Wu Q, Liu K, Wang L, Li S, Gao W, Zhang L, Zheng H, Li Z, Hao J. Recent decrease trend of atmospheric mercury concentrations in East China: The influence of anthropogenic emissions. Atmos. Chem. Phys. 2018; 18: 8279-8291.

Tokos JJS, Hall B, Calhoun JA, Prestbo EM. Homogeneous gas-phase reaction of Hg° with H2O2, 03, CH3I, AND (CH3)2S: Implications for atmospheric Hg cycling. Atmos. Environ. 1998; 32: 823-827.

Tong Y, Eichhorst T, Olson MR, McGinnis JE, Turner I, Rutter AP, Shafer MM, Wang X, Schauer JJ. Atmospheric photolytic reduction of Hg (II) in dry aerosols. Environ. Sci. Proc. Imp. 2013; 15: 1883-1888.

Tong Y, Eichhorst T, Olson MR, Rutter AP, Shafer MM, Wang X, Schauer JJ. Comparison of heterogeneous photolytic reduction of Hg (II) in the coal fly ashes and synthetic aerosols. Atmos. Res. 2014; 138: 324-329.

Travnikov O, Angot H, Artaxo P, Bencardino M, Bieser J, D'Amore F, Dastoor A, De Simone F, DIéguez MC, Dommergue A, Ebinghaus R, Feng XB, Gencarelli CN, Hedgecock IM, Magand O, Martin L, Matthias V, Mashyanov N, Pirrone N, Ramachandran R, Read KA, Ryjkov A, Selin NE, Sena F, Song S, Sprovieri F, Wip D, Wangberg I, Yang X. Multi-model study of mercury dispersion in the atmosphere: atmospheric processes and model evaluation. Atmos. Chem. Phys. 2017: 5271-5295.

UNEP. Global Mercury Assessment 2018. United Nations Environment Program, Geneva, Switzerland, 2019.

Urba A, Valiulis D, Šarlauskas J, Kvietkus K, Šakalys J, Selskis A. A pilot study of different materials applied for active sampling of gaseous oxidized mercury in the atmospheric air. Atmos. Pollut. Res. 2017.

Vijayaraghavan K, Karamchandani P, Seigneur C, Balmori R, Chen SY. Plume-in-grid modeling of atmospheric mercury. J. Geophys. Res. Atmos. 2008; 113.

Vijayaraghavan K, Stoeckenius T, Ma L, Yarwood G, Morris R, Levin L. Analysis of temporal trends in mercury emissions and deposition in Florida. 10th International Conference on Mercury as a Global Pollutant. Halifax, NS, Canada, pp. MG4A-O10.

Wang C, Wang Z, Hui F, Zhang X. Speciated atmospheric mercury and sea–air exchange of gaseous mercury in the South China Sea. Atmos. Chem. Phys. 2019; 19: 10111-10127.

Wang F, Saiz-Lopez A, Mahajan A, Martín JG, Armstrong D, Lemes M, Hay T, Prados-Roman C. Enhanced production of oxidised mercury over the tropical Pacific Ocean: a key missing oxidation pathway. Atmos. Chem. Phys. 2014a; 14: 1323.

Wang S, Schmidt JA, Baidar S, Coburn S, Dix B, Koenig TK, Apel E, Bowdalo D, Campos TL, Eloranta E, Evans MJ, DiGangi J, Zondlo M, Gao RS, Haggerty JA, Hall SR, Hornbrook RS, Jacob DJ, Morley B, Pierce B, Reeves M, Romashkin P, Ter Schure A, Vlokamer R. Active and widespread halogen chemistry in the tropical and subtropical free troposphere. Proc. Natl. Acad. Sci. U. S. A. 2015; 112: 9281-9286.

Wang X, Bao Z, Lin CJ, Yuan W, Feng X. Assessment of Global Mercury Deposition through Litterfall. Environ. Sci. Technol. 2016; 50: 8548-8557.

Wang Y, Liu R, Li Y, Cui X, Zhou J, Liu S, Zhang Y. GEM in the marine atmosphere and air-sea exchange of Hg during late autumn and winter cruise campaigns over the marginal seas of China. Atmos. Res. 2017; 191: 84-93.

Wang Y, Peng Y, Wang D, Zhang C. Wet deposition fluxes of total mercury and methylmercury in core urban areas, Chongqing, China. Atmos. Environ. 2014b; 92: 87-96.

Warnick SL, Bell HL. The acute toxicity of some heavy metals to different species of aquatic insects. J. Water Pollut. Control Fed. 1969; 41: 280-284.

Weigelt A, Ebinghaus R, Manning AJ, Derwent RG, Simmonds PG, Spain TG, Jennings SG, Slemr F. Analysis and interpretation of 18 years of mercury observations since 1996 at Mace Head, Ireland. Atmos. Environ. 2015; 100: 85-93.

Weigelt A, Ebinghaus R, Pirrone N, Bieser J, Bödewadt J, Esposito G, Slemr F, Van Velthoven PFJ, Zahn A, Ziereis H. Tropospheric mercury vertical profiles between 500 and 10 000 m in central Europe. Atmos. Chem. Phys. 2016; 16: 4135-4146.

Weiss-Penzias P, Amos H, Selin N, Gustin M, Jaffe D, Obrist D, Sheu G-R, Giang A. Use of a global model to understand speciated atmospheric mercury observations at five high-elevation sites. Atmos. Chem. Phys. 2015; 15: 1161-1173.

Weiss-Penzias P, Coale K, Heim W, Fernandez D, Oliphant A, Dodge C, Hoskins D, Farlin J, Moranville R, Olson A. Total-and monomethyl-mercury and major ions in coastal California fog water: Results from two years of sampling on land and at sea. Elem. Sci. Anth. 2016a; 4.

Weiss-Penzias P, Gustin MS, Lyman SN. Observations of speciated atmospheric mercury at three sites in Nevada: Evidence for a free tropospheric source of reactive gaseous mercury. J.Geophys.Res. 2009; 114: D14302.

Weiss-Penzias P, Sorooshian A, Coale K, Heim W, Crosbie E, Dadashazar H, MacDonald AB, Wang Z, Jonsson H. Aircraft Measurements of Total Mercury and Monomethyl Mercury in Summertime Marine Stratus Cloudwater from Coastal California, USA. Environ. Sci. Technol. 2018; 52: 2527-2537.

Weiss-Penzias PS, Gay DA, Brigham ME, Parsons MT, Gustin MS, ter Schure A. Trends in mercury wet deposition and mercury air concentrations across the US and Canada. Sci. Total Environ. 2016b; 568: 546-556.

Weiss-Penzias PS, Gustin MS, Lyman SN. Sources of gaseous oxidized mercury and mercury dry deposition at two southeastern US sites. Atmos. Environ. 2011; 45: 4569-4579.

Weiss-Penzias PS, Ortiz C, Acosta RP, Heim W, Ryan JP, Fernandez D, Collett JL, Flegal AR. Total and monomethyl mercury in fog water from the central California coast. Geophys. Res. Lett. 2012; 39.

White EM, Keeler GJ, Landis MS. Spatial variability of mercury wet deposition in eastern Ohio: summertime meteorological case study analysis of local source influences. Environ. Sci. Technol. 2009; 43: 4946-4953.

White EM, Landis MS, Keeler GJ, Barres JA. Investigation of mercury wet deposition physicochemistry in the Ohio River Valley through automated sequential sampling. Sci. Total Environ. 2013; 448: 107-119.

Wright LP, Zhang L, Cheng I, Aherne J, Wentworth GR. Impacts and effects indicators of atmospheric deposition of major pollutants to various ecosystems-A review. Aerosol Air Qual. Res. 2018; 18: 1953-1992.

Wright PL, Zhang L, Marsik FJ. Overview of mercury dry deposition, litterfall, and throughfall studies. Atmos. Chem. Phys. 2016; 16: 13399-13416.

Wu Q, Wang S, Li G, Liang S, Lin CJ, Wang Y, Cai S, Liu K, Hao J. Temporal trend and spatial distribution of speciated atmospheric mercury emissions in China during 1978−2014. Environ. Sci. Technol. 2016; 50: 13428-13435.

Xiu G, Cai J, Zhang W, Zhang D, Büeler A, Lee S, Shen Y, Xu L, Huang X, Zhang P. Speciated mercury in size-fractionated particles in Shanghai ambient air. Atmos. Environ. 2009; 43: 3145-3154.

Xu X, Liao Y, Cheng I, Zhang L. Potential sources and processes affecting speciated atmospheric mercury at Kejimkujik National Park, Canada: Comparison of receptor models and data treatment methods. Atmos. Chem. Phys. 2017; 17: 1381-1400.

Xu X, Yang X, Miller DR, Helble JJ, Carley RJ. Formulation of bi-directional atmosphere-surface exchanges of elemental mercury. Atmos. Environ. 1999; 33: 4345-4355.

Yan Y, Pozzer A, Ojha N, Lin J, Lelieveld J. Analysis of European ozone trends in the period 1995-2014. Atmos. Chem. Phys. 2018; 18: 5589-5605.

Ye Z, Mao H, Lin CJ, Youn Kim S. Investigation of processes controlling summertime gaseous elemental mercury oxidation at midlatitudinal marine, coastal, and inland sites. Atmos. Chem. Phys. 2016; 16: 8461-8478.

Yin X, Kang S, Foy Bd, Ma Y, Tong Y, Zhang W, Wang X, Zhang G, Zhang Q. Multi-year monitoring of atmospheric total gaseous mercury at a remote high-altitude site (Nam Co, 4730 m asl) in the inland Tibetan Plateau region. Atmos. Chem. Phys. 2018; 18: 10557-10574.

Yin Y, Chen B, Mao Y, Wang T, Liu J, Cai Y, Jiang G. Possible alkylation of inorganic Hg (II) by photochemical processes in the environment. Chemosphere 2012; 88: 8-16.

Yu G, Qin X, Xu J, Zhou Q, Wang B, Huang K, Deng C. Characteristics of particulate-bound mercury at typical sites situated on dust transport paths in China. Sci. Total Environ. 2019; 648: 1151-1160.

Yu Q, Luo Y, Wang S, Wang Z, Hao J, Duan L. Gaseous elemental mercury (GEM) fluxes over canopy of two typical subtropical forests in south China. Atmos. Chem. Phys. 2018; 18: 495-509.

Zhang H, Feng X, Larssen T, Qiu G, Vogt RD. In inland China, rice, rather than fish, is the major pathway for methylmercury exposure. Environ. Health Perspect. 2010; 118: 1183-1188.

Zhang L, Blanchard P, Gay DA, Prestbo E, Risch M, Johnson D, Narayan J, Zsolway R, Holsen T, Miller E. Estimation of speciated and total mercury dry deposition at monitoring locations in eastern and central North America. Atmos. Chem. Phys. 2012a; 12: 4327-4340.

Zhang L, Blanchard P, Johnson D, Dastoor A, Ryzhkov A, Lin C, Vijayaraghavan K, Gay D, Holsen T, Huang J. Assessment of modeled mercury dry deposition over the Great Lakes region. Environ. Pollut. 2012b; 161: 272-283.

Zhang L, Jaffe DA. Trends and sources of ozone and sub-micron aerosols at the Mt. Bachelor Observatory (MBO) during 2004–2015. Atmos. Environ. 2017; 165: 143-154.

Zhang L, Lyman S, Mao H, Lin C-J, Gay DA, Wang S, Sexauer Gustin M, Feng X, Wania F. A synthesis of research needs for improving the understanding of atmospheric mercury cycling. Atmos. Chem. Phys. 2017a; 17: 9133-9144.

Zhang L, Wang L, Wang S, Dou H, Li J, Li S, Hao J. Characteristics and sources of speciated atmospheric mercury at a coastal site in the East China Sea region. Aerosol Air Qual. Res. 2017b; 17: 2913-2923.

Zhang L, Wright LP, Blanchard P. A review of current knowledge concerning dry deposition of atmospheric mercury. Atmos. Environ. 2009; 43: 5853-5864.

Zhang Y, Jacob DJ, Horowitz HM, Chen L, Amos HM, Krabbenhoft DP, Slemr F, Louis VLS, Sunderland EM. Observed decrease in atmospheric mercury explained by global decline in anthropogenic emissions. Proc. Natl. Acad. Sci. U. S. A. 2016; 113: 526-531.

Zhang Y, Jaeglé L. Decreases in mercury wet deposition over the United States during 2004–2010: Roles of domestic and global background emission reductions. Atmosphere 2013; 4: 113-131.

Zhang Y, Jaeglé Lv, Donkelaar Av, Martin R, Holmes C, Amos H, Wang Q, Talbot R, Artz R, Brooks S. Nested-grid simulation of mercury over North America. Atmos. Chem. Phys. 2012c; 12: 6095-6111.

Zhao H, Yan H, Zhang L, Sun G, Li P, Feng X. Mercury contents in rice and potential health risks across China. Environ. Int. 2019; 126: 406-412.

Zhou H, Hopke PK, Zhou C, Holsen TM. Ambient mercury source identification at a New York State urban site: Rochester, NY. Sci. Total Environ. 2019; 650: 1327-1337.

Zhou H, Zhou C, Hopke PK, Holsen TM. Mercury wet deposition and speciated mercury air concentrations at rural and urban sites across New York state: Temporal patterns, sources and scavenging coefficients. Sci. Total Environ. 2018a; 637-638: 943-953.

Zhou H, Zhou C, Lynam MM, Dvonch JT, Barres JA, Hopke PK, Cohen M, Holsen TM. Atmospheric Mercury Temporal Trends in the Northeastern United States from 1992 to 2014: Are Measured Concentrations Responding to Decreasing Regional Emissions? Environ. Sci. Technol. Lett. 2017a; 4: 91-97.

Zhou J, Wang Z, Zhang X. Deposition and Fate of Mercury in Litterfall, Litter, and Soil in Coniferous and Broad-Leaved Forests. J. Geophys. Res. Biogeosci. 2018b; 123: 2590-2603.

Zhou J, Wang Z, Zhang X, Sun T. Investigation of factors affecting mercury emission from subtropical forest soil: A field controlled study in southwestern China. J. Geochem. Explor. 2017b; 176: 128-135.

Zhu W, Lin CJ, Wang X, Sommar J, Fu X, Feng X. Global observations and modeling of atmosphere-surface exchange of elemental mercury: A critical review. Atmos. Chem. Phys. 2016; 16: 4451-4480.

Zhu W, Sommar J, Lin CJ, Feng X. Mercury vapor air-surface exchange measured by collocated micrometeorological and enclosure methods - Part II: Bias and uncertainty analysis. Atmos. Chem. Phys. 2015; 15: 5359-5376.